A Journal of the Gesellschaft Deutscher Chemiker

Angewandte International Edition

GDCh

Chemie

www.angewandte.org

Accepted Article

Title: Solar-to-Fuels: Recent Advances in Light-driven C1 Chemistry

Authors: Guangbo Chen, Geoffrey I.N. Waterhouse, Run Shi, Jaiqing Zhao, Zhenhua Li, Li-Zhu Wu, Chen-Ho Tung, and Tierui Zhang

To be cited as: *Angew. Chem. Int. Ed.* 10.1002/anie.201814313
Angew. Chem. 10.1002/ange.201814313

Link to VoR: http://dx.doi.org/10.1002/anie.201814313
http://dx.doi.org/10.1002/ange.201814313

WILEY-VCH

10.1002/anie.201814313

Solar-to-Fuels: Recent Advances in Light-driven C1 Chemistry

Guangbo Chen,[a, d] Geoffrey I.N. Waterhouse,[c] Run Shi,[a] Jiaqing Zhao,[a] Zhenhua Li,[a] Li-Zhu Wu,[a] Chen-Ho Tung,[a] and Tierui Zhang*[a, b]

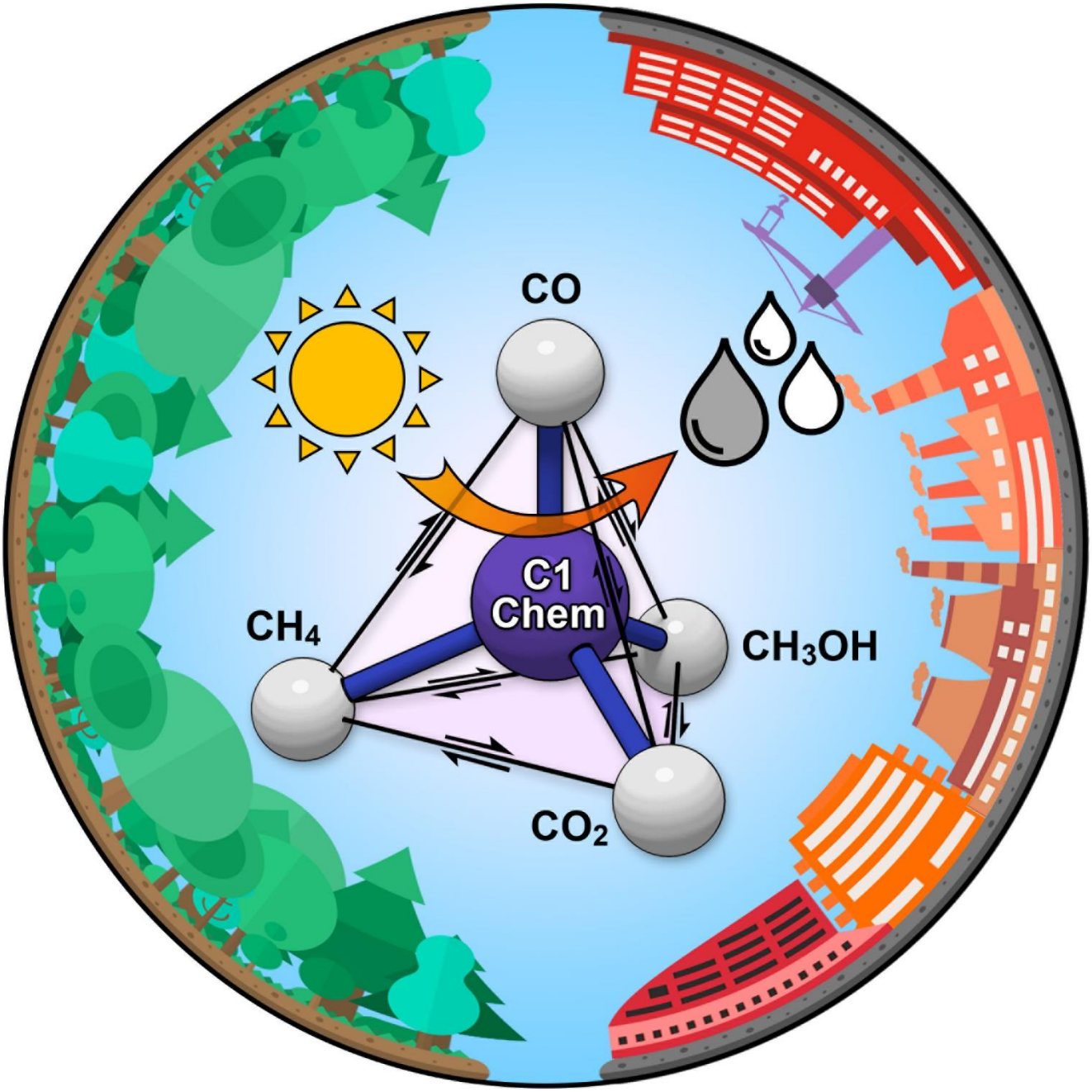

Abstract: Catalytic C1 chemistry based on the activation/conversion of synthesis gas (CO + H_2), methane, carbon dioxide and methanol offers great potential for the sustainable development of hydrocarbon fuels to replace oil, coal and natural gas. Traditional thermal catalytic processes used for C1 transformations require high temperatures and pressures, thereby carrying a significant carbon footprint. In comparison, solar-driven C1 catalysis represents a greener and more sustainable pathway for the manufacturing of fuels and other commodity chemicals, though conversion efficiencies are currently too low to justify industry investment. In this review, we highlight recent advances and milestones in light-driven C1 chemistry, including solar Fischer-Tropsch synthesis, water-gas-shift reaction, CO_2 hydrogenation, methane and methanol conversion reactions. Particular emphasis is placed on the rational design of catalysts, structure-reactivity relationships as well as reaction mechanisms. Strategies for the scaling up of solar-driven C1 processes are also discussed.

1. Introduction

1.1. An Overview of C1 Chemistry

Today's chemical industry is heavily reliant on fossil fuels for the manufacture of commodity chemicals and as energy sources. However, this dependence on fossil fuels as a feedstock in chemical syntheses is not sustainable since fossil fuel reserves are limited. Further, burning fossil fuels for energy releases CO_2 into the atmosphere, with CO_2 emissions from the chemical industry and derived transportation fuels being major contributors to total anthropogenic emissions and therefore a direct cause of global warming.[1, 2, 3, 4] In order to reduce the dependency on oil and other fossil fuels in the chemical sector, considerable research effort has been devoted over the past two decades to the development of novel catalytic technologies for transforming C1 building blocks into fuels and other high value chemicals.[5, 6] C1 chemistry refers to the conversion of small molecules with only one carbon atom, including compounds such as carbon monoxide (CO), carbon dioxide (CO_2), methane (CH_4) or methanol (CH_3OH), into premium products with high demand.[7, 8] C1 chemistry can also be used to produce high-purity hydrogen or premium specialty chemicals from synthesis gas or methanol.[9] Typically, the C1 building blocks originate from coal, natural gas, biomass or organic wastes.[10] Catalytic processes used in C1 conversion include the Fischer-Tropsch synthesis (FTs), water-gas-shift (WGS) reaction, CO_2 hydrogenation reaction, CH_4 conversion and methanol reforming. Recently, great advances have been made in the development of solar-driven versions of these traditional thermal catalytic processes, especially in areas such as catalyst fabrication, mechanistic understanding and reactor design,[11, 12, 13, 14] which are discussed in detail below.

[a] G. Chen, Dr. R. Shi, J. Zhao, Z. Li, Prof. L.-Z. Wu, Prof. C.-H. Tung, Prof. T. Zhang
Key Laboratory of Photochemical Conversion and Optoelectronic Materials, Technical Institute of Physics and Chemistry, Chinese Academy of Sciences, Beijing 100190, P. R. China
Tel: +86 10 82543428 Fax: +86 10 62554670
E-mail: tierui@mail.ipc.ac.cn (T. Zhang)
[b] Prof. T. Zhang
Center of Materials Science and Optoelectronics Engineering, University of Chinese Academy of Sciences, Beijing 100049, P. R. China
[c] Prof. G. I.N. Waterhouse
School of Chemical Sciences, the University of Auckland, Auckland 1142, New Zealand
[d] G. Chen
Center for Advancing Electronics Dresden and Department of Chemistry and Food Chemistry, Technische Universität Dresden, Dresden 01062, Germany

1.2. Catalytic CO conversion: Fischer-Tropsch synthesis and Water-Gas-Shift Reaction

Heterogeneous catalytic conversion of carbon-rich resources such as coal, natural gas, and biomass-derived syngas (CO+H_2) into clean fuels and valuable chemicals *via* the FTs is of great economic importance due to the growing global demand for liquid hydrocarbon fuels that have traditionally been obtained from petroleum.[15, 16] FTs yields a wide distribution of liquid hydrocarbon fuels, olefins, waxes and oxygenated compounds (**Figure 1**).[17, 18] Extensive research effort has been devoted to developing more efficient FTs catalysts, with enhanced activity, product selectivity and catalyst stability being the main foci.[11, 19] Typical catalysts used for FTs are Ru, Fe, Co and Ni. Amongst these catalysts, Ni favors methane generation due its strong hydrogenation ability.[20] Ru is the most active metal for FTs, able to work at low temperatures (<150°C) whilst showing good selectivity to long-chain hydrocarbons. Co-based catalysts are generally quite active and show good selectivity for the production of linear long-chain hydrocarbons, such as waxes and diesel fuels.[21] Fe-based catalysts are suitable for the production of linear alkanes and also the production of alkenes or oxygenates.[18, 22] In addition to the catalyst, the nature of catalyst support,[23, 24] the type of promoter,[25, 26] the reactor type,[27] and the operating conditions[28] also have a significant influence on catalytic activity and product selectivity.[11]

The WGS reaction ($CO + H_2O \rightarrow CO_2 + H_2$) is an indispensable process in the chemical industry for hydrogen production and carbon monoxide removal.[29] Iron oxide-based catalysts are widely used for the high-temperature WGS reaction (operating temperature range of 350-450 °C).[30] Cu, Ce and Cr promoters have been shown to improve the activity and stability of iron oxide-based catalysts for the WGS reaction.[31, 32, 33] Au-based catalysts and copper-zinc-oxide-based catalysts are used for the low temperature WGS reaction (operating temperature range of 200-300 °C), showing high activity and good selectivity.[34, 35, 36]

1.3. CO_2 Conversion

Anthropogenic CO_2 emissions arising from the combustion of fossil fuels for the production of electricity and transportation are the primary cause of global warming. CO_2 capture and storage (CCS)[8, 37] and CO_2 conversion[38, 39] are emerging technologies for reducing CO_2 emissions. In particular, catalytic CO_2 hydrogenation represents arguably the most important and practical pathway for large-scale CO_2 utilization (Figure 1).[12, 40] Catalysts developed to date for CO_2 hydrogenation are typically based on supported Fe, Co, Ni, Cu, Rh or Ru (and their combinations), with the product distribution controlled by the unique electronic structure at catalytic active sites.[41] Depending on the catalyst(s) used and the reaction conditions, production distributions can be tuned towards various products, including carbon monoxide, methane, higher hydrocarbons, methanol, higher alcohols, dimethyl ether or formate species.[41, 42, 43]

Catalytic conversion of CO_2 to CO *via* the reverse water-gas shift (RWGS) reaction ($CO_2 + 2H_2 \rightarrow CO + 2H_2O$) has attracted considerable attention. Cu-based catalysts such as Cu/ZnO, Cu–Zn/Al_2O_3 and Cu/SiO_2 that are commonly used in WGS are also active in RWGS due to the reversibility of the reaction.[44, 45]

The complete catalytic hydrogenation of CO_2 to methane, also called the Sabatier reaction ($CO_2 + H_2 \rightarrow CH_4 + 2H_2O$), is another important catalytic pathway for CO_2 conversion.[46] A number of catalytic systems based on VIII-B metals (e.g. Ru and Rh) supported by oxides have been studied for the CO_2 methanation reaction.[8, 47]

Compared to CO_2 methanation, catalytic CO_2 hydrogenation to longer chain hydrocarbons is much more attractive, though technically more challenging.[12] Hydrocarbon production pathways by CO_2 hydrogenation can be divided into two categories: methanol-mediated and non-methanol-mediated approaches.[40, 48] In the methanol-mediated approach, CO_2 and H_2 react over Cu-Zn-based catalysts to produce methanol, which is subsequently transformed into other hydrocarbons through the methanol reforming process. In the case of non-methanol-mediated pathway, CO_2 hydrogenation proceeds *via* two steps: RWGS reaction and then FTs.[49]

For the generation of methanol *via* catalytic CO_2 hydrogenation, the most widely used catalysts are copper (Cu)-based and gallium (Ga)-based. The benchmark catalyst employed in industry for methanol synthesis is Cu/ZnO/Al_2O_3, which employs a $CO/CO_2/H_2$ feed.[50] Other recently reported catalysts for methanol synthesis using CO_2 as the carbon feedstock include Cu/CeO_x/TiO_2,[51] NiGa alloy,[52] and $GaPd_2$ alloy nanoparticles (NPs).[53, 54, 55]

1.4. CH_4 Conversion

Methane is the main component in natural gas and methane clathrates. Accordingly, it is a very important hydrocarbon feedstock for the synthesis of fuels and other commodity chemicals. In addition, commercial production of H_2 is based primarily on catalytic steam reforming (along with partial oxidation and coal gasification technologies), making the CH_4 conversion of great fundamental and practical importance to the chemical industry (**Figure 2**).

The non-oxidative coupling of methane (NOCM) reaction to generate ethane and ethylene is a highly desirable approach towards these valuable compounds, though thermodynamically unfavorable. Generally, the reaction occurs *via* a two-step process. Firstly, methane is chemisorbed on the surface of catalyst. Second, the cleavage of C-H bonds occurs, resulting in the formation of H_2 and H-deficient carbon intermediates such as CH_x.[56] When the CH_x coverage on the surface of the catalyst is high, C-C coupling reactions occur. Pt/SiO_2 was the first catalyst found to be active for the NOCM reaction.[57] The methane dehydroaromatization (MDA) reaction is another pathway for the non-oxidative conversion of methane, first reported in 1993.[58] The combination of Mo and ZSM-5 was found to be very active for MDA.[59] In 2014, Bao et al. made a great breakthrough in NOCM over a highly dispersed Fe/silica catalyst.[60] At high temperatures (1363 K), methane was converted to ethylene with a selectivity of 48.4% at 48.1% conversion of methane, with the balance of the products being aromatics and hydrogen.

The complete oxidation of methane (COM, $CH_4 + 2O_2 \rightarrow CO_2 + 2H_2O$) is thermodynamically favorable but the products are low value. In comparison with the complete oxidation process, the partial oxidation of methane (POM) to oxygenates is far more attractive from a catalysis viewpoint, especially if control of the CH_4 conversion and product selectivity is desired.[61] For example, the POM to methanol, which can be directly used in fuel cells, is highly desirable.[62] Various homogeneous catalysts have been reported to catalyze methane oxidation to methanol, including Pt,[63, 64], Hg[65] and Pd[66, 67, 68] complexes. Heterogeneous catalysts can also convert methane to methanol, such as Fe[69, 70, 71] and Cu[72, 73] anchored on zeolites. In this process, high reaction temperatures (400-800 K) and pressures (20-70 bar) are needed to achieve meaningful methane conversion rates. Very recently, a colloidal PdAu catalyst,[74] supported Rh catalysts[76] and a graphene-confined single atom Fe catalyst[75] were developed

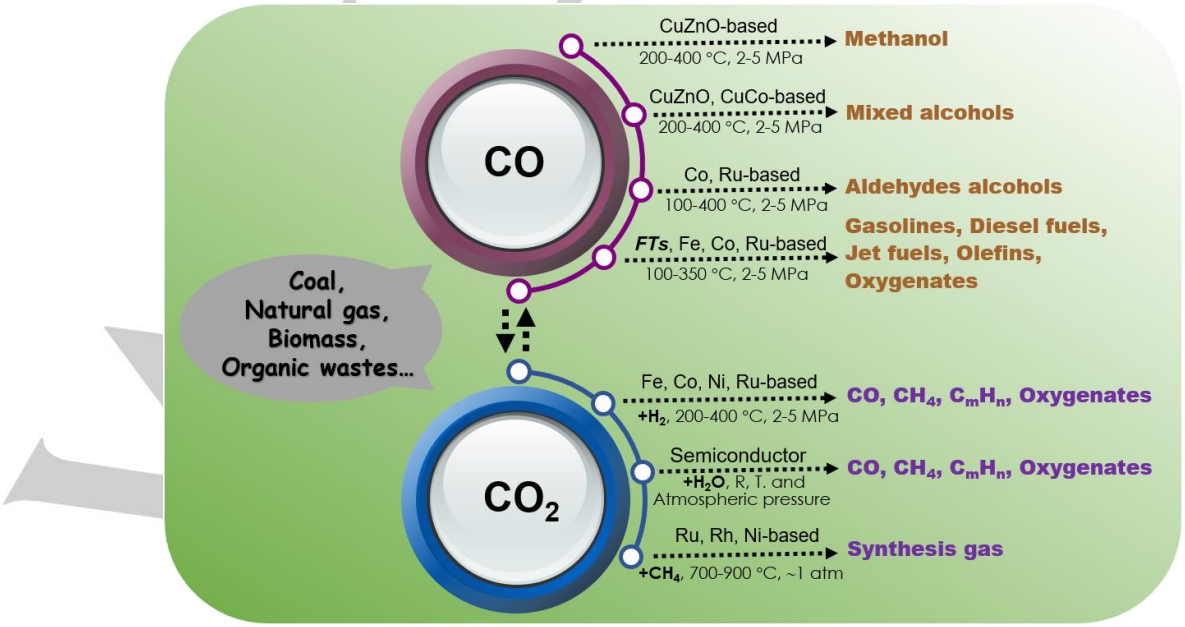

Figure 1. Catalytic pathways for CO and CO_2 conversion.

which could efficiently convert CH_4 to methanol even at low temperatures.

The steam reforming of methane (SRM, $CH_4 + H_2O \rightarrow CO + 3H_2$) is widely employed to produce syngas for methanol synthesis and hydrogen. Dry reforming of methane (DRM) using CO_2 as the oxidizer ($CH_4 + CO_2 \rightarrow 2CO + 2H_2$) is advantageous as a means of mitigating greenhouse gases emissions and reducing CH_4 consumption. With regard to reforming catalysts, initial research focused mainly on noble metal catalysts such as Rh, Ir, Pt, Ru and Pd, with Ru and Rh being the most active.[76] Subsequently, non-precious metal Ni-based catalysts were developed that demonstrated superior catalytic activity in these reforming reactions.[77] Moreover, CH_3X (X = F, Cl, Br or I) and CS_2 can be also produced *via* methane oxidation when X_2 or sulfur are used as oxidants, respectively.[78, 79]

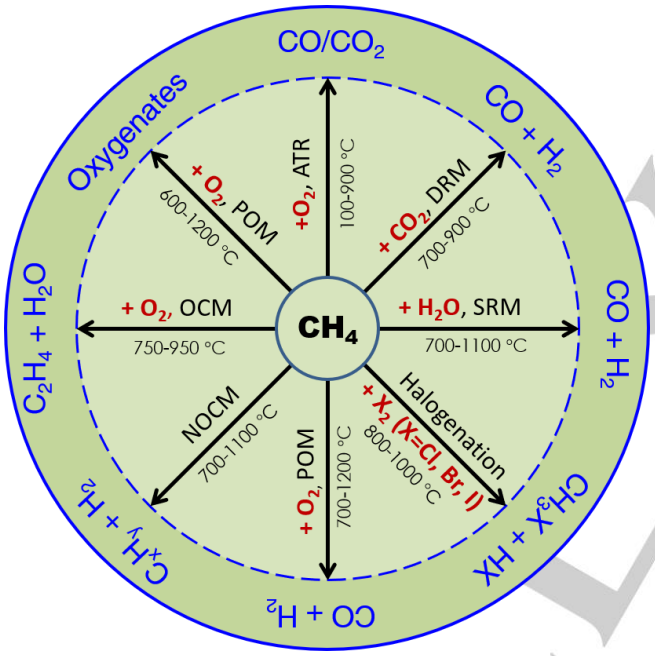

Figure 2. The catalytic pathways for methane conversion. ATR: autothermal reforming, DRM: dry reforming of methane, SRM: steam reforming of methane, POM: partial oxidation of methane, NOCM: non-oxidative coupling of methane OCM: oxidative coupling of methane.

1.5. CH_3OH Conversion

CH_3OH is the simplest alcohol and can be readily produced from a variety of carbon sources such as natural gas, shale gas, coal, biomass and carbon dioxide.[10] Methanol itself can be directly used as an alternative fuel for commercial applications, such as methanol-fueled cars and methanol fuel cells. Moreover, methanol also represents a promising energy carrier as a hydrogen storage material (it is 12.6 wt.% hydrogen). Importantly, methanol can be converted to hydrogen at relatively low temperatures (150-350°C) *via* aqueous-phase methanol reforming ($CH_3OH + H_2O \rightarrow CO_2 + H_2$). The energy input required for methanol reforming is much lower than that required to reform methane or other hydrocarbons with C-C bonds (>500°C). To date, the benchmark catalysts for methanol reforming are Pt/Al_2O_3,[80] $Cu/Zn/Al_2O_3$-based,[81] Pt/α-MoC[82] catalysts, as well as the homogenous catalyst $[RuHCl(CO)(HN(C_2H_4PiPr_2)_2)]$,[83] which operate in the temperature range 65-300°C. The Pt/α-MoC catalyst developed by Ma's group demonstrated superb catalytic activity for hydrogen production *via* methanol reforming, with a turn-over-frequency (TOF) of 18046 h^{-1} at low-temperatures (150-190 °C).[82] Other valuable chemicals, such as formaldehyde, acetic acid and olefins can be also produced from methanol, with direct methanol C-C bond coupling reactions arguably the most attractive and challenging aspect of methanol chemistry.[84] Amongst C-C coupling reactions, the methanol-to-olefins (MTO) process represents a key future technology for transforming coal or natural gas into the key feedstocks needed by the plastics industry.[85] Many companies and research institutions (especially the Dalian Institute of Chemical Physics) have put great effort into developing the MTO reaction by systematically exploring catalyst synthesis,[86, 87, 88] reaction mechanisms[14, 89] and process engineering.[90, 91] To date, the most commonly used MTO catalysts are acid zeolite-based catalysts, with the reaction mechanism involving organic species confined in the zeolite pores, which act as intermediates in the formation C-C bonds *via* methylation and production of water, followed by acid-catalyzed cracking to generate olefins. Long chain olefins can undergo dehydrocyclization, resulting in the formation of aromatics and paraffins.[92]

1.6. Light-driven C1 Chemistry: a Green and Sustainable Approach

The discussion above highlights progress to date in thermal catalytic C1 chemistry. However, many of the reactions of interest demand harsh temperature and pressure conditions. Hence, alternative low-energy input technologies are needed to make C1 chemistry more sustainable. Compared with traditional thermal technologies, solar-driven C1 chemistry is promising alternative approach which makes use of abundant and clean solar energy.[93] In the past decade, great progress has been made in light-driven C1 conversions, especially in processes such as light-driven FTs, WGS, CO_2 reduction, CH_4 and CH_3OH conversion. Within these reactions, the photocatalytic CO_2 conversion using H_2O as hydrogen source over semiconductor photocatalysts is especially attractive ($CO_2 + H_2O \rightarrow CO$, CH_4, etc.), though conversion rates are typically low (falling in the ~mmol h^{-1} range). The photocatalytic reaction is initiated by the generation of electron−hole carriers under light excitation. The charge carriers, once spatially separated, migrate to the surface of the photocatalyst and react with adsorbed acceptor molecules, thereby promoting CO_2 reduction and H_2O oxidation processes.[94] A number of excellent review articles have already been published relating to photocatalytic CO_2 reduction[95, 96] and photoelectrochemical CO_2 reduction[97, 98], examining both photocatalysts design and reaction mechanisms. Accordingly, the CO_2 conversion section of this review focusses mainly on light-driven CO_2 hydrogenation reactions. In this context, key aspects of catalyst design, structure-activity relationships and reaction mechanisms during the light-driven processes will be examined. Further, advanced techniques relating to catalyst characterization will also be discussed (**Figure 3**). We aim to provide a state-of-the-art update regarding the development of highly efficient C1 conversion catalysts, hinting at the potential of such catalytic systems for future CO_2 conversion and industrial applications.

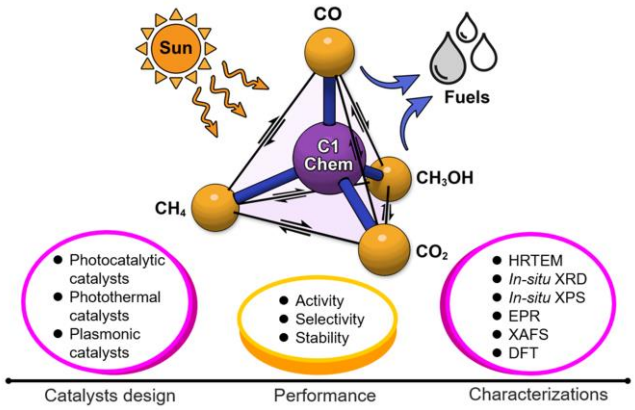

Figure 3. Schematic illustration of light-driven C1 chemistry.

2. Light-driven CO conversion

2.1 Light-driven Fischer-Tropsch synthesis

Dai and co-workers first discovered that UV light could efficiently promote the methanation of CO over Ru/TiO_2.[105] Later, Guo et al. dispersed worm-like ruthenium nanostructures on graphene sheets and found that the resulting catalyst could efficiently drive FTs to hydrocarbons (C_2-C_4: ~15%, C_{5+}: 82%) under mild conditions (150 °C) and visible light irradiation.[99] The catalytic conversion rate reached as high as 14.4 $mol_{CO}{\cdot}mol_{Ru}^{-1}{\cdot}h^{-1}$ and could be further enhanced by increasing the light intensity or decreasing the light wavelength. The apparent activation energy for the FTs under light irradiation was approximately 56 kJ mol^{-1}, which was much lower than the value for the same reaction in the dark (~72 kJ mol^{-1}). Results conclusively demonstrate that light irradiation can effectively reduce the activation energy barrier for FTs (**Figure 4**).

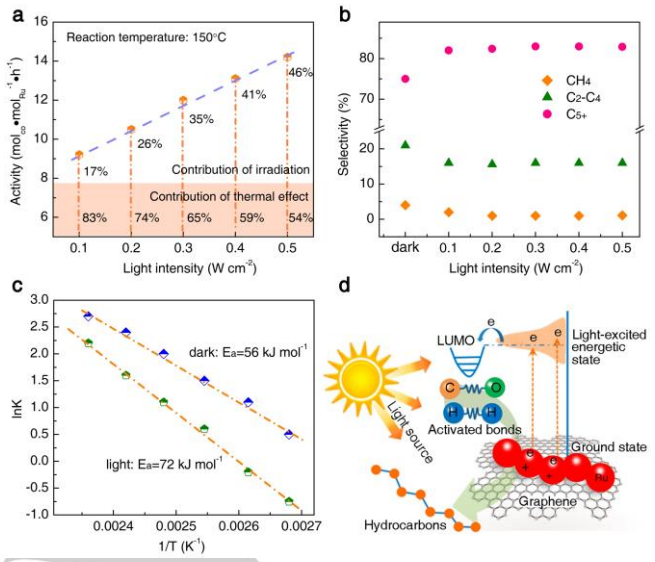

Figure 4. a, b) Dependence of catalytic activity and selectivity, respectively, of Ru/graphene for photocatalytic FTs. c) Arrhenius plots of light-induced FTs reaction and the dark catalytic reaction. d) Schematic showing the reaction process FTs over Ru/graphene under light irradiation. Reproduced with permission.[99] Copyright 2015, American Chemical Society.

Subsequently, Ni catalysts and various Group VIII metal-containing catalysts were developed, all of which showed ~100% selectivity to CH_4 for CO hydrogenation.[100] Balancing hydrogenation and C-C coupling reactions is of great importance from a fundamental scientific viewpoint and also an industrial perspective. Very recently, Zhang et al fabricated a series of Ni-based catalysts by reduction of pre-calcined NiAl-layered double hydroxide (LDH) nanosheets at 525 °C in a H_2 atmosphere. The obtained Ni-based catalysts afforded an unexpectedly high selectivity to C_{2+} hydrocarbons during the FTs reaction under light irradiation.[101] Following UV-vis light irradiation for 45 min, the CO conversion reached 27.7% with a C_{2+} selectivity of 58.5%. Moreover, the same Ni-based catalyst demonstrated excellent catalytic activity under visible-light irradiation. *In-situ* X-ray diffraction (XRD), *in-situ* X-ray photoelectron spectroscopy (XPS), X-ray absorption fine structure (XAFS) and transmission electron microscopy (TEM) analyses revealed that alumina-supported Ni^0 NPs partially decorated with nickel oxide overlayers were responsible for the formation of the C_{2+} hydrocarbons (**Figure 5a-e**). Density function theory (DFT) calculations further determined that the modification of metallic Ni by the surface oxides changed the reaction pathway of surface CH_x intermediates towards higher hydrocarbons, making the novel Ni-based catalyst system very efficient for C-C coupling during the FTs (Figure 5f, g). However, in this system, C_2-C_4 alkanes were the main reaction products, which are much less valuable than alkenes or longer chain hydrocarbons (C_{5+}). Achieving the ideal balance between hydrogenation and C-C coupling is a huge challenge in the development of light-driven FTs catalysts.

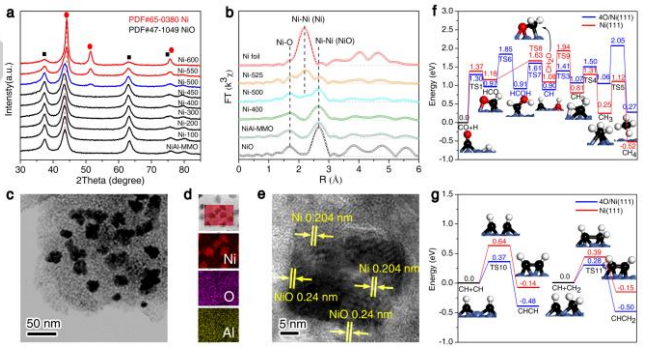

Figure 5. a) *In-situ* XRD patterns for NiAl-MMO and Ni-*x*, where *x* is the H_2 reduction temperature. b) EXAFS of NiAl-MMO and Ni-*x*. c) Annular bright-field (ABF) scanning TEM (STEM) image, d) Element maps for Ni-525. e) High-resolution TEM (HRTEM) image. The potential-energy profile of the most possible reaction paths for syngas conversion on Ni(111) and 4O/Ni(111), f) CH_4 formation. g) C-C coupling. Reproduced with permission.[101] Copyright 2016, Wiley-VCH.

Using metals with mild hydrogenation ability such as Co, is an effective strategy for tuning FTs catalyst selectivity towards olefins. Reduction of ZnCoAl-LDH nanosheets at 300-700 °C afforded a series of photothermal catalysts for light-driven FTs, with the performance of the catalysts depending on the reduction temperature (**Figure 6a**).[102] Under UV-vis irradiation, a photothermal catalyst prepared at 450 °C (denoted as Co-450) demonstrated remarkable FTs performance for the production of light olefins (C_2-$C_4^=$) with a selectivity of 36%. Characterization studies using XAFS and HRTEM revealed that the active catalyst consisted Co and Co_3O_4 NPs on a ZnO-Al_2O_3 mixed metal oxide

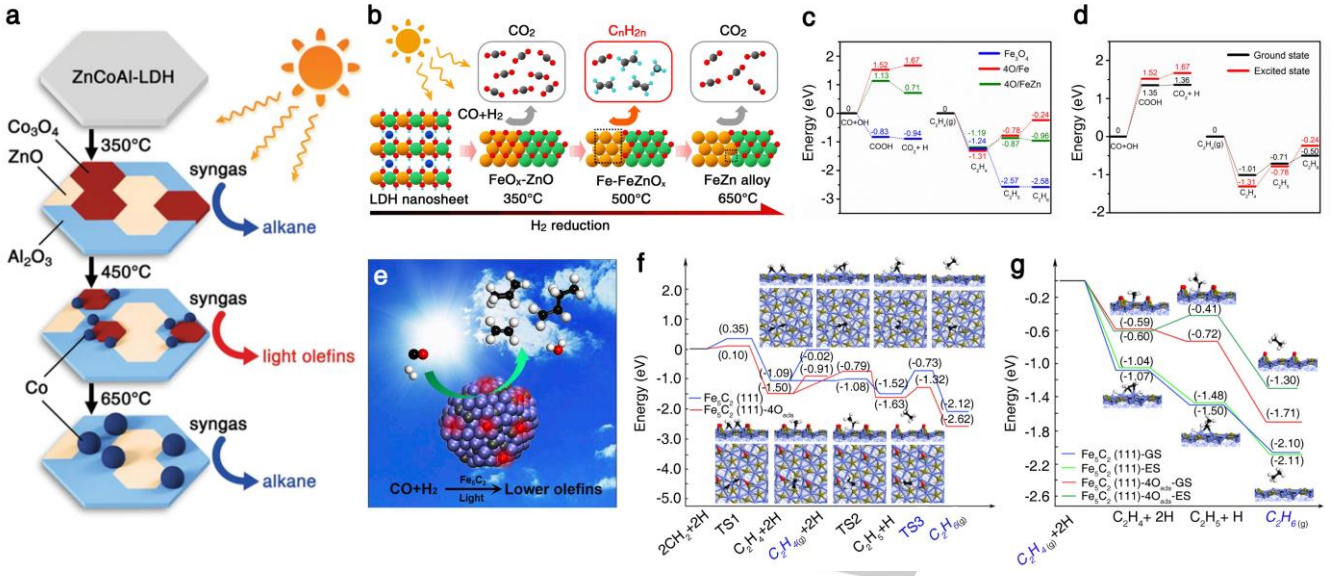

Figure 6. a) Fabrication of Co-*x* catalysts and their light-driven FTs performance. Reproduced with permission.[102] Copyright 2018, Wiley-VCH. b) Reductive transformation of ZnFeAl-LDH nanosheets to Fe-x catalysts and their photocatalytic behavior in FTs. Energy profiles for CO_2 formation, C_2H_4 adsorption, and hydrogenation under: c) excited states on Fe_3O_4, 4O/Fe, and 4O/Fe_3Zn, and d) ground states and excited states (thermal- and photodriven catalysis) on 4O/Fe. Reproduced with permission.[103] Copyright 2018, Wiley-VCH. e) Photocatalytic FTs performance over oxygen-decorated Fe_5C_2. f) Energy profiles for CH_2 coupling and hydrogenation to C_2H_6 on Fe_5C_2(111) and Fe_5C_2(111)-$4O_{ads}$. g) Energy profiles for C_2H_4 adsorption and hydrogenation to C_2H_6 under ground state and excited state conditions on Fe_5C_2(111)-$4O_{ads}$ and Fe_5C_2(111) surfaces. Reproduced with permission.[104] Copyright 2018, Elsevier.

(ZnAl-MMO) support. DFT calculations demonstrated that the oxide-decorated metallic Co NPs heterostructure lessened the hydrogenation ability of Co^0, thereby allowing C-C coupling reactions with a high selectivity to light olefins. Due to the relatively high price of Co, Fe has been widely pursued as a low cost catalyst for FT to olefins (FTO) both in academia and industry settings. Fe-based catalysts, such as FeO_x-modified Fe^0[103] and oxygen-decorated Fe_5C_2[104] heterostructures, display excellent FTO activity under light irradiation. For example, after H_2 reduction of ZnFeAl-LDH nanosheets at 500°C, the obtained catalyst (Fe-500) comprising of Fe^0 and FeO_x NPs on a ZnAl-MMO support demonstrated remarkable CO hydrogenation performance with very high initial selectivity toward hydrocarbons (89%) and especially light olefins (42%). The intimate and abundant interfacial contacts between metallic Fe^0 and FeO_x in the Fe-500 photocatalyst contributed its outstanding photocatalytic performance (Figure 6b). Excited state DFT simulations were used investigate differences in reaction between ground state thermal catalysis and exited state photo-driven catalysis. As shown in Figure 6c, d, CO_2 formation under ground state conditions requires less energy input than under exited state conditions. Conversely, ethene interacted more strongly with surface under the excited state conditions, with further hydrogenation to ethane demanding significantly more energy input, highlighting the advantage of photocatalytic olefin synthesis. Furthermore, Ma et al. demonstrated the light could change the FTO pathway over Fe_5C_2 catalyst, resulting in an olefin/paraffin (O/P) ratio of 10.9 with CO conversion >49% (Figure 6e, f). XAFS and XPS studies revealed that under light-irradiation, the surface of the Fe_5C_2 catalyst was partly decorated by O-atoms generated *in-situ*, leading to a high selectivity towards olefins. These studies demonstrate a number of fascinating light-driven platforms for the production of light olefins through CO hydrogenation. Additionally, these catalysts operated equally well in batch tests and flow reactor tests, the latter suggesting great potential for industry uptake.

Table 1 summarizes recent advances in light driven FTs. It is evident from the data that light-driven FTs is still very much in the developmental stage. Further studies aimed at optimizing catalyst design and clarifying reaction mechanisms are needed to expedite the development of light-driven FTs.

2.2 Light-driven Water-Gas-Shift Reaction

Garcia et al. discovered that noble metal NPs loaded on TiO_2 or CeO_2 could simultaneously catalyze H_2O reduction to H_2 and CO oxidation to CO_2.[105] Under simulated solar irradiation, Au/TiO_2 showed the highest activity with H_2 and CO_2 production rates of 10506 μmol $g^{-1}_{cat.}$ and 13447 μmol $g^{-1}_{cat.}$, respectively. The molar stoichiometry of evolved CO_2 and H_2 in the early stages of the photocatalytic reaction was approximately 1:1, in accordance with expectations for the WGS reaction (**Figure 7a**). Control experiments suggested that UV photons were responsible for the photocatalytic activity of these particular catalysts. Two photocatalytic mechanisms were proposed depending on the energy of the excitation photons (Figure 7b). In the first mechanism, UV photons could directly excite TiO_2, resulting in the charge separation. Subsequently, the electrons in the conduction band of the semiconductor migrated onto the noble metal NPs, which acted as the co-catalyst to facilate water reduction. Holes in the valence band of TiO_2 oxidized CO to CO_2. In the second mechanism, excitation of surface plasmon of Au NPs under visible light irradiation resulted in the injection of hot electrons into conduction band of the TiO_2 to drive water reduction, whilst holes on the Au NPs were responsible for the oxidation of CO.

Table 1. Performance of various catalysts in light-driven FTs.

Catalysts	Feed (CO/H_2)	Reactor type	P (MPa)	Temperature (°C)	Light source	CO conversion (%)	CO_2 selectivity (%)	C_xH_y selectivity (%, CO_2-free)				O/P[a]	Ref
								CH_4	$C_{2-4}^=$	C_{2-4}^o	C_{5+}		
Ru/TiO_2	1:40	flow	100 mL min^{-1}	180+ solar	300 W Xe lamp	~100	-	100	0	0	0	0	[106]
Ru/Graphene	1:2	batch	3.0	150+ solar	300 W Xe lamp	43	-	2.6	15.7	81.7	-	-	[99]
Ni/TiO_2	1:3	flow	100 mL min^{-1}	250+ solar	300 W Xe lamp	~100	0	100	0	0	0	0	[107]
$Ni\text{-}NiO/Al_2O_3$	1:3	batch	0.18	solar	300 W Xe light	27.7 (45 min)	2.7	38.8	<1	37.4	21.1	~0	[101]
30% Co/TiO_2 nanotube	1:2	batch	2.0	220+ solar	500 W Hg lamp	17.1 (55 h)	8.4	31.5	31.7	0.8	36.0	0.02	[108]
$Co\text{-}Co_3O_4$/ZnAl-MMO	1:3	batch	0.18	solar	300 W Xe light	15.4 (1 h)	47.6	48.0	36.0	5.9	10.1	6.1	[102]
$Co\text{-}Co_3O_4$/ZnAl-MMO	1:3	flow	5 mL min^{-1}	solar	300 W Xe light	13 (20 h)	-	~42	~38	6.5	13.5	5.9	[102]
$Fe\text{-}Fe_3O_4$/ZnAl-MMO	1:3	batch	0.18	solar	300 W Xe light	20.9 (2 h)	20.9	28.6	42.4	9.0	8.6	4.7	[103]
$Fe\text{-}Fe_3O_4$/ZnAl-MMO	1:3	flow	5 mL min^{-1}	solar	300 W Xe light	11.4 (20 h)	7.1	37.7	40.0	6.6	8.6	6.1	[103]
Fe_5C_2	1:2	batch	-	solar	300 W Xe lamp	49.5 (0.5 h)	18.9	33.1	55.5	5.1	6.3	10.9	[104]

[a] olefin/paraffin ratio;

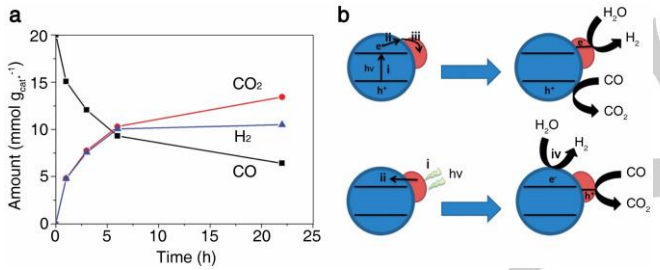

Figure 7. a) Temporal profile of CO consumption, CO_2 evolution and H_2 evolution over a Au/TiO_2 (1 wt.%) catalyst under solar light irradiation. b) Two possible mechanisms used to rationalize the UV-visible and visible light photocatalytic activity of Au/TiO_2. Reproduced with permission.[105] Copyright 2013, Royal Society of Chemistry.

3. Light-driven CO_2 Hydrogenation

3.1. Light-driven Reverse Water-Gas-Shift Reaction

Light-driven RWGS was firstly reported over a ZrO_2 photocatalyst.[109] Fourier-transform infrared spectroscopy (FTIR) results revealed that the CO_2 was first adsorbed on ZrO_2 in the form of a carbonate in the dark, followed by the reduction of carbonate into formate under light irradiation[110] Electron paramagnetic resonance (EPR) and blank experiments indicated that H_2 was activated in the dark and then reacted with a photoexcited CO_2^- radical to generate formate.[111] The formate acted as a reducing agent for the transformation of gaseous CO_2 into CO.[112, 113] Ga_2O_3[114] and alkaline perovskites ($ATiO_3$, A = Li, Na or K) are also active for the light-driven RWGS reaction.[115]

Regarding photocatalysts for the RWGS reaction, TiO_2 favors the production of CH_4 and other alkanes, whereas the addition of In or In/Cu co-catalysts boosts the CO selectivity.[116] Similar effects were seen for $NiO\text{-}In_2O_3/TiO_2$ materials.[117] Recently, Ozin et al. reported that $In_2O_{3-x}(OH)_y$ NPs demonstrated excellent activity for the photocatalytic reduction of CO_2 with H_2 under both ultraviolet and visible light.[118] In a batch reactor operated at 150 °C, CO generation rates reached as high as 0.25 μmol g_{cat}^{-1} h^{-1} and 70 nmol g_{cat}^{-1} h^{-1} under simulated solar and visible light ($\lambda > 420$ nm) illumination, respectively. Experimental results and DFT calculations determined that the surface populations of oxygen vacancies and hydroxides played a significant role in the photocatalytic RWGS process. Inspired by the exciting results seen for $In_2O_{3-x}(OH)_y$, it was subsequently discovered that the oxidizing strength of the precursor anion had a critical effect on the population of surface defect sites, thereby influencing the final photocatalytic activity[119] (**Figure 8a**). Assembling $In_2O_{3-x}(OH)_y$ nanocrystals into porous nanorods superstructures[120] or integration of $In_2O_{3-x}(OH)_y$ with vertically aligned silicon nanowires (SiNW)[121] further promotes photocatalytic RWGS activity (Figure 8b, c). Time dependent density functional theory (TPDFT) calculations results found that surface frustrated Lewis pairs (SFLPs) created by Lewis acid coordinatively unsaturated surface indium sites proximal to an oxygen vacancy became more acidic, and a Lewis basic surface hydroxide site in $In_2O_{3-x}(OH)_y$ become more basic, in the excited state compared to the ground state (Figure 8d, e).[122] Femtosecond transient absorption measurements further revealed that oxygen vacancies and surface hydroxyl groups played a significant role in the excited-state charge relaxation pathways, which strongly correlated to photocatalytic activity.[123] Moreover, experimental results and DFT calculations demonstrated that the photocatalytic CO_2 reduction performance of $In_2O_{3-x}(OH)_y$ could be greatly enhanced through isomorphous substitution of In^{3+} with Bi^{3+}[124] (Figure 8d-j). Deep understanding of the role and function surface defects in controlling surface acidity/basicity and charge carrier dynamics over $In_2O_{3-x}(OH)_y$ catalyst provides a framework for the rational design of more efficient catalysts for CO_2 reduction, as well as other solar energy-conversion-related catalytic reactions including FTs and CH_4 conversion.

Owing to its high abundance, non-toxicity and low cost, silicon has recently emerged as an attractive semiconductor for converting sunlight into electricity.[125] Ozin et al. found that hydride-terminated silicon (ncSi:H) nanocrystals with average diameter 3.5 nm could serve as a single component heterogeneous reducing agent for converting CO_2 to CO at a rate of hundreds of mmol h^{-1} g^{-1} (**Figure 9a**). FTIR analysis indicated that the Si-H surface sites contributed strongly to the conversion of CO_2 to CO (Figure 9b). EPR and the temperature studies revealed that the enhanced conversion rate of CO_2 under light irradiation was due to a photothermal effect (Figure 9c, d). DFT calculations further suggested the surface SiH were the most

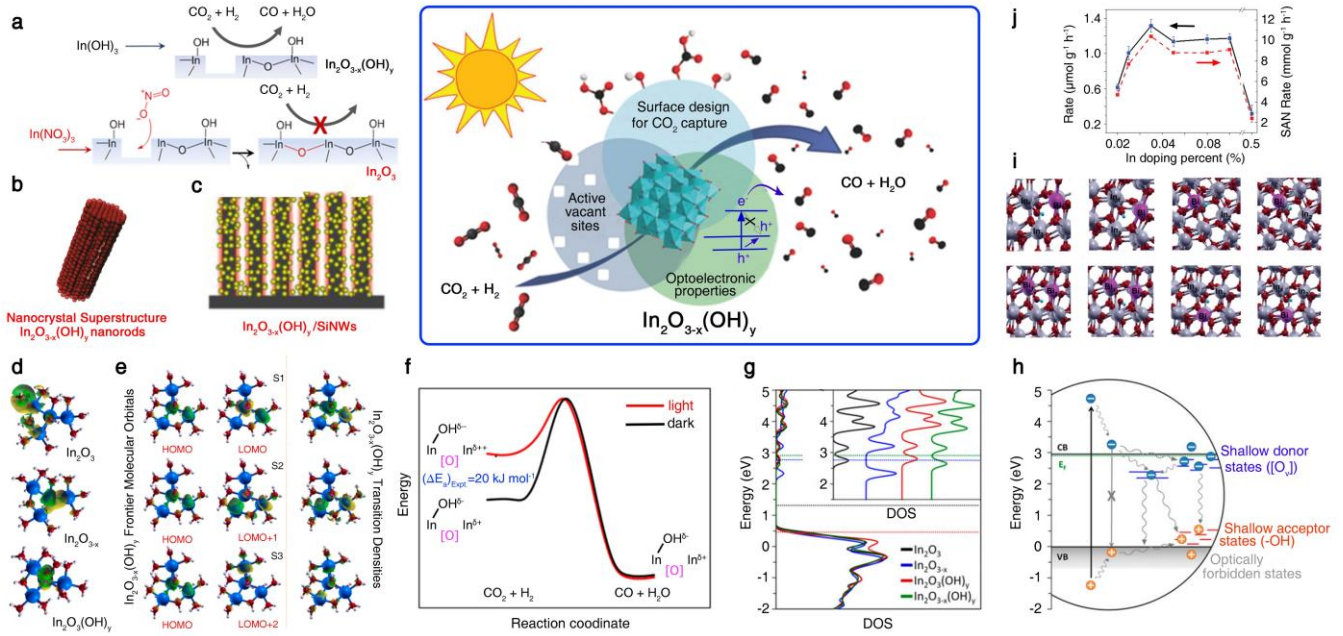

Figure 8. $In_2O_{3-x}(OH)_y$ for light-driven RWGS. a) Effect of precursor on the photocatalytic performance. b) $In_2O_{3-x}(OH)_y$ nanocrystal superstructures, c) $In_2O_{3-x}(OH)_y$ nanocrystal superstructures coated on SiNWs. d) Representative transition densities for the S1 excited states of pristine In_2O_3, defected In_2O_{3-x} and defected $In_2O_3(OH)_y$ surfaces. e) Visualization of the main contributing molecular orbitals and transition densities. Reproduced with permission.[119, 120, 121, 122] Copyright 2016, American Chemical Society. f) Schematic illustration of the origin of the difference in the experimental activation energy $(\Delta E_a)_{Expt.}$ for the RWGS reaction involving the GS surface FLP in the dark and ES surface FLP in the light. g, h) Comparison between calculated total DOS for pristine and defected (111) indium oxide surfaces and a schematic diagram illustrating the different charge carrier relaxation processes in $In_2O_{3-x}(OH)_y$. Reproduced with permission.[123] Copyright 2016, National Academy of Sciences. i) Initial and final configurations of the surface with Bi substitution at different sites. j) Plot of average CO production rate (black) and surface-normalized CO production rate as a function of the Bi doping level. Reproduced with permission.[124] Copyright 2018, Wiley-VCH.

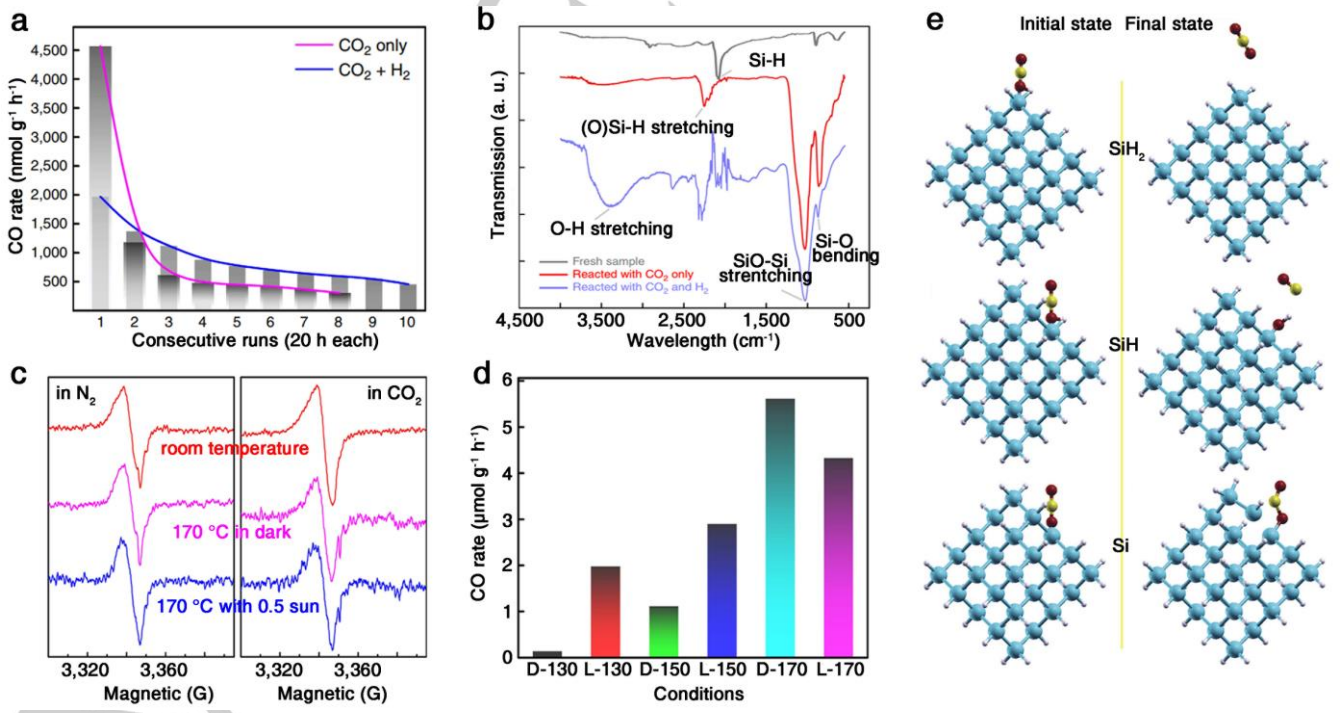

Figure 9. a) CO production rates over ncSi:H in a batch reactor at 150 °C. b) FTIR study of surface properties. c) EPR spectra of ncSi:H samples under different conditions. d) CO production rates of three ncSi:H film tested at different heating temperatures. e) The initial models and the final optimized models for CO_2 adsorption on SiH_2, SiH and Si surface sites. Reproduced with permission.[126] Copyright 2017, Nature Publishing Group.

favorable sites for CO_2 reduction on ncSi:H catalysts (Figure 9e).

Photo-assisted catalysis mediated by the local surface plasmon resonance (LSPR) of plasmonic nanometals has also become a fascination of researchers in the field of solar-to-chemical-energy conversion.[127, 128] Plasmonic excitation of Au NPs on a ZnO support could result in significant heating of the Au/ZnO catalyst and conversion of CO_2 and H_2 to CO and CH_4.[129] Changing the support from ZnO to TiO_2 or CeO_2 further enhanced the catalytic performance due to a greatly decreased apparent activation energy.[130] Further, light irradiation could also effectively modulate the interface interaction of Pt-MoO_x[131] and Au-MoO_x[132] to promote the RWGS activity.

Recently, photothermal catalysts have become popular for the light-driven RWGS reaction. Ye et al. found that the Fe NPs loaded on Al_2O_3 showed excellent RWGS activity *via* a photothermal effect.[133] Furthermore, carbon layer-coated Fe (Fe@C) catalysts exhibited excellent catalytic performance in the solar-driven RWGS in comparison with naked Fe NPs (Fe/SiO_2 or Fe/CNT) (**Figure 10a-c**).[134] *In situ* monitoring of the catalyst temperature during the reaction revealed that photo-irradiation induced a significant thermal heating effect, which was responsible for the high activity. Electromagnetic-field simulation results indicated that plasmon-photon coupling was amplified at the surface of Fe NPs, resulting in enhanced generation of energetic hot electrons for CO_2 activation. DFT calculations determined that the carbon shell on the Fe NPs promoted the desorption of CO from the catalyst surface, thereby explaining the very high reaction selectivity of the Fe@C catalyst for CO_2 hydrogenation to CO (Figure 10d, e). Ozin and co-workers recently demonstrated that the RWGS reaction could also be driven by a visible and near-infrared responsive Pd@Nb_2O_5 catalyst.[135] Taking advantage of photothermal effects, Pd@Nb_2O_5 efficiently hydrogenated CO_2 to CO at an impressive rate of 1.8 mmol g_{cat}^{-1} h^{-1}. The photothermal effect was determined to originate from intraband and/or interband optical excitation and nonradiative relaxation of Pd nanocrystals. The mechanism of this photothermal process involved H_2 dissociation on Pd nanocrystals and subsequent spillover of H onto the Nb_2O_5 nanorods whereupon adsorbed CO_2 was hydrogenated to CO.

In addition to precious metals and transition metals, low cost aluminum (Al) also has outstanding plasmonic optical properties, including a highly size-tunable localized plasmon resonance that can range from the UV to the visible region.[136] Halas et al. demonstrated a plasmonic Al@Cu_2O antenna-reactor heterostructure that could efficiently drive the RWGS under very mild operating conditions.[137] Theoretical investigations using the finite element method (FEM) and Monte-Carlo simulations suggested a plasmon-induced carrier generation mechanism was driving the RWGS under light irradiation, wherein Al acted as a plasmonic antenna to promote reactivity on the adjacent semiconducting Cu_2O shell. The antenna-reactor Al@Cu_2O nanostructure thus not only improves surface reactivity, but efficiently harnesses and utilizes the radiative LSPR damping in Al to enhance carrier generation in Cu_2O.

3.2. Light-driven CO_2 Methanation

Photocatalytic CO_2 methanation was first reported by Gratzel et al. using Ru/RuO_x/TiO_2 materials.[138] Under light irradiation, the conversion of CO_2 to CH_4 was observed and a significant temperature increase from ambient to 46 °C also noted. A later study revealed that thermal effects caused by light irradiation contributed to the methanation process.[139] Continuing the theme of using Ru for light-driven CO_2 methanation, Ozin et al. recently reported the photo-methanation of CO_2 over small Ru NPs sputtered onto black SiNWs.[140] Under concentrated solar illumination (~15 suns), the Ru/SiNWs afforded a CH_4 production rate of 1 mmol g^{-1} h^{-1}. The authors also performed comparative tests to distinguish thermal and radiative effects. It was found that the reaction rates were highly dependent on the photon flux and wavelength range at a constant temperature (93 °C). Moreover, rate enhancements with heating were more marked under light irradiation, even though activation energies (and thus, mechanistic routes) appeared were determined to be identical under light and thermal only heating regimes. Therefore, it was concluded that the conversion pathway under light irradiation involved a photocatalytic process. It is expected that the catalytic activity of this system could be enhanced by orders of magnitude through optimizing the size, distribution, and loading of the Ru NPs over the support, as well as increasing the solar intensity.[141] Apart from Ru, various transition metal nanomaterials also show excellent activity for CO_2 methanation under light irradiation (rates on the order of a few mol h^{-1} g^{-1}).[133] The catalytic activities are highly dependent on the metal, and decrease in the order Ru > Rh > Ni > Co > Pd > Pt > Ir > Fe. Temperature monitoring reveals that substantial heating can occur upon light irradiation, a phenomenon which is explained by the photothermal effect of the metal NPs. Experimental tests in the dark and under visible light verified that the conversion behavior of the aforementioned group VIII metals was due to a photothermal effect (**Figure 11a-c**). In order to improve photothermal catalytic CO_2 methanation activity, simultaneous activation of CO_2 and H_2 is necessary. Based on this requirement, Ye et al. embedded Ru NPs in exfoliated LDH nanosheets (Ru@FL-LDHs), which showed very high catalytic activity for CO_2 methanation under light irradiation in both batch and flow reactors (Figure 11d-g).[142] The excellent catalytic performance over the Ru/FL-LDHs catalyst originated mainly from the specific activation of CO_2 and H_2 over exfoliated LDHs and Ru NPs, respectively.

Further investigations of Group VIII metallic nanomaterials determined that plasmonic Rh NPs were also photocatalytic, simultaneously lowering activation energies and product selectivity in CO_2 hydrogenation.[143] The selectivity of CO_2 hydrogenation over a Rh/Al_2O_3 catalyst differed depending on whether the reaction was run under thermal or photo-driven conditions. The apparent activation energies (E_a) of the thermo- and photo-reactions for CO production were 64.7 and 50.4 kJ mol^{-1}, respectively, indicating the light-induced hot electrons could efficiently lower the energy barrier for the CO_2 conversion process (**Figure 12**a, b). DFT calculations were carried out to understand how hot electrons affect the intermediates in the rate-determining-step (RDS) of CH_4 and CO production. As summarized in Figure 12c, in the thermocatalytic process, phonons activate both CHO and CO intermediates and produce CH_4 and CO at comparable rates. In the light-driven process, the hot electrons are selectively transferred into the anti-bonding orbitals of the CHO intermediates to weaken the chemical bonds and drive the reaction on a charged-state reaction coordinate characterized by a reduced activation energy, resulting in the high selectivity toward CH_4 production.

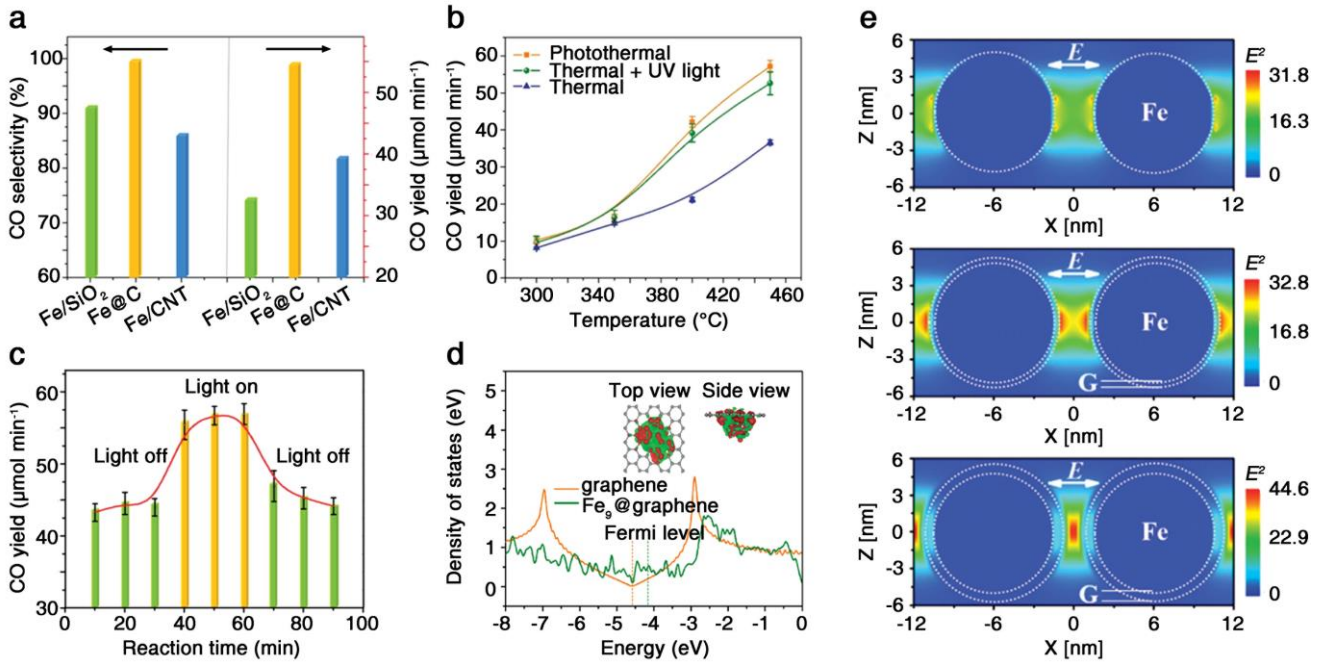

Figure 10. Photo-induced thermo-catalytic CO_2 conversion performance of Fe@C, Fe/SiO_2 and Fe/CNT catalysts. b) Comparison of CO evolution rates for the light-induced thermal and traditional thermal CO_2 hydrogenation over the Fe@C catalyst c) CO evolution rates at 450 °C with and without UV-light illumination over Fe@C catalyst. d) Projected density of states for the pz orbitals of C atoms bonded with Fe atoms in a Fe9@graphene model in comparison with C atoms in a pristine graphene model. e) Spatial distribution of the SPR-induced enhancement of electric field intensity at the SPR peak wavelength (350 nm), from finite-difference-time-domain (FDTD) simulation of 9 nm Fe NPs, 9 nm Fe NPs coated with a single carbon layer, and 9 nm Fe NPs coated by multiple carbon layers. Reproduced with permission.[134] Copyright 2016, Wiley-VCH.

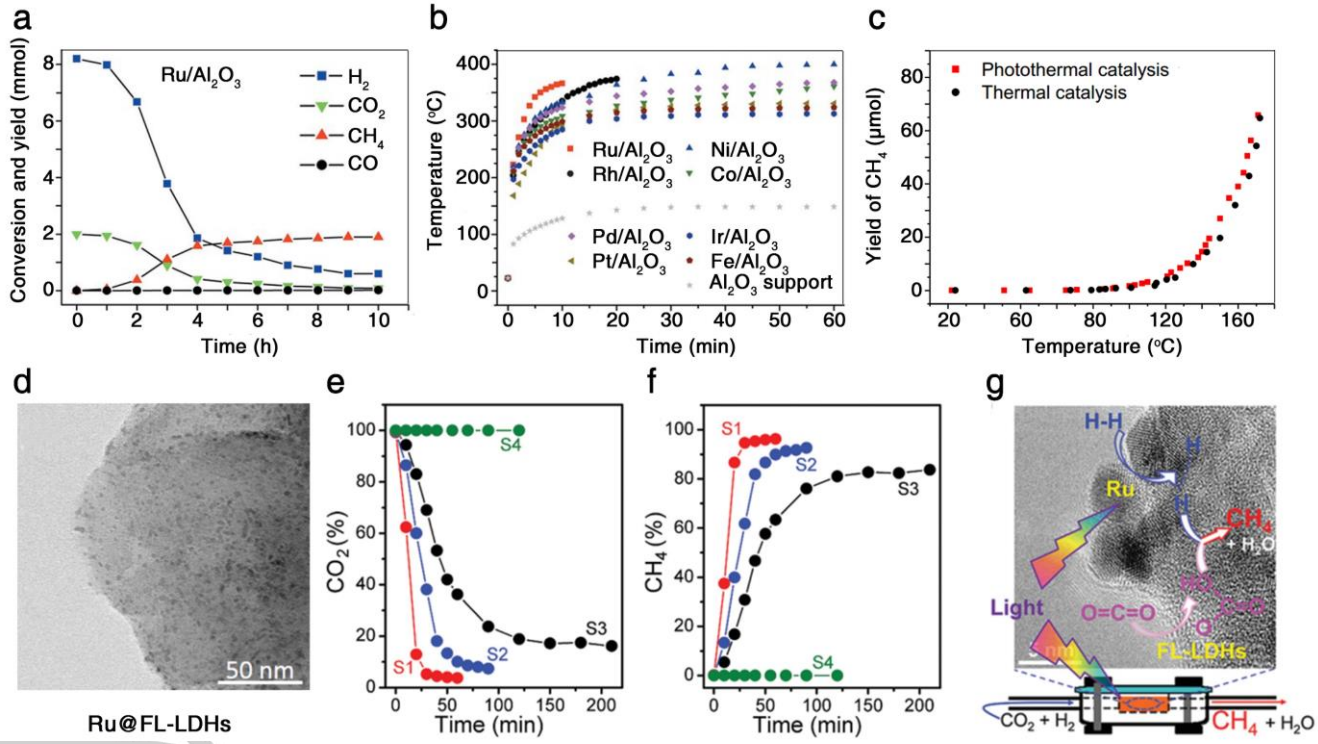

Figure 11. Photothermal CO_2 conversion on a Ru/Al_2O_3 catalyst. b) Monitoring of the catalyst temperature as a function of light irradiation time. c) CH_4 evolution over Ru/Al_2O_3 catalyst under photothermal and conventional thermal catalysis conditions. Reproduced with permission.[133] Copyright 2014, Wiley-VCH. d) TEM image of Ru/FL-LDHs, e) CO_2 reactant and f) CH_4 product in photothermal conversion of CO_2 over Ru-based catalysts, S1: Ru@FL-LDHs, S2: Ru@LDHs, S3: $Ru@SiO_2$, S4: FL-LDHs. g) Schematic showing the simultaneous activation of CO_2 and H_2, as well as the hydrogenation process, over Ru@FL-LDHs. Reproduced with permission.[142] Copyright 2016, Wiley-VCH.

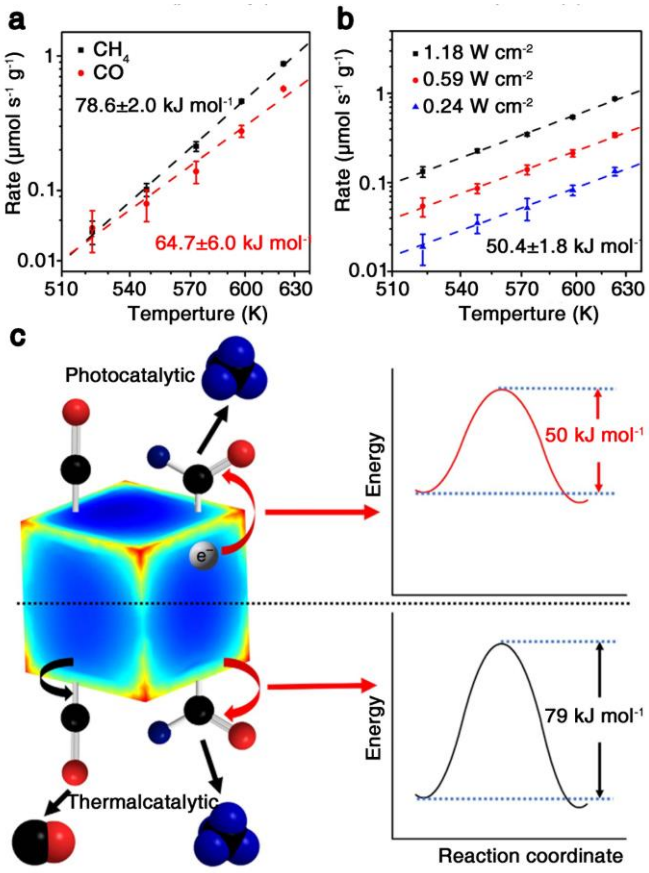

Figure 12. a) Thermal-catalytic reaction rates of CH_4 and CO production on Rh/Al_2O_3 as a function of temperature. The apparent activation energies are obtained by fitting the results to an Arrhenius equation. b) Photoreaction rates for CH_4 production on Rh/Al_2O_3 under different light intensities as a function of temperature. c) Reaction mechanism for CO and CH_4 evolution on a rhodium nanocube. Reproduced with permission.[143] Copyright 2017, Nature Publishing Group.

Although superior activities have been achieved for light driven CO_2 methanation over the Group VIII metallic nanomaterials, especially supported-Ru catalysts, debate continues about the catalytic mechanism and whether photocatalytic or photothermal processes dominate. Thus, it is necessary to distinguish the catalytic mechanism in further research. Particularly, *in-situ* techniques such as Raman spectra and EPR should be adopted to monitor the local temperature and detect the photo-excited carriers.

3.3. Light-driven Methanol Production

Izumi et al. discovered that zinc- and Zn/Cu-based LDHs containing carbonate anions ($[Zn_{3-x}Cu_xM^{III}(OH)_8]_2[CO_3]\cdot mH_2O$, where M^{III} = Al or Ga) were promising photocatalysts for CO_2 hydrogenation to methanol under UV-vis light irradiation.[144] Further, methanol production rates and methanol selectivity could be enhanced by replacing inter-layer carbonate with $[Cu(OH)_4]^{2-}$ anions in Zn-Ga or Zn-Cu-Ga LDH materials.[145] *In situ* Cu K-edge X-ray absorption near edge structure and FTIR analyses were applied to study the reaction mechanism for methanol synthesis on these LDHs materials.[146] Firstly, CO_2 reacted with a hydroxy group bounded to interlayer Cu^{II} to form hydrogen carbonate. Next, a forbidden direct e-transition from an O 2p orbital to M 3d (M = Zn, Ga) occurred, followed by photo-generated electrons and holes in the LDHs being transferred to the Cu^{II} sites and H atom, respectively. Finally, the trapped electrons on Cu^{I} were transferred to the hydrogen carbonate resulting in the formation of anionic hydrogen carbonate. In order to improve the photoactivity of CO_2 reduction, WO_3 and CuZnGa-LDH were successfully integrated into a reverse polymer electrolyte photo-fuel cell.[147] Under UV-visible excitation, WO_3 photoxidized H_2O to O_2, with CuZnGa-LDH reducing CO_2 to CH_3OH. Additionally, Ag was found to be an efficient cocatalyst for accelerating CO_2 photoreduction and enhancing CH_3OH selectivity *via* a plasmonic effect.[148]

A further investigation showed that the defect-laden In_2O_3, $In_2O_{3-x}(OH)_y$, could efficiently photo-catalyze the hydrogenation of CO_2 to methanol (**Figure 13**a, b).[149] In a flow reactor system operating at atmospheric pressure and 250 °C, methanol production at 97.3 and 54.1 mmol g_{cat}^{-1} h^{-1} (methanol selectively >50%) was observed with and without UV-vis illumination, respectively. DFT calculations suggested that hydrogen was split heterolytically by the surface hydroxide of InOH (Lewis base site) and the In surface (Lewis acid site), resulting in $InOH_2$ and In-H, respectively. Next, H*-assisted formation of intermediates including HCO_2*, H_2CO_2* and CH_3O* occurred (panel II- panel V). The addition of a final proton completed the mechanism in panel (VI), resulting in the desorption of methanol and water, with the overall process being slightly exothermic (~209 kJ mol^{-1}) (Figure 13c). DFT calculations highlighted the role of the unique surface configuration in the reaction, with light irradiation contributing to the catalytic process by enhancing the reactivity of the SFLP site for hydrogen activation.[122]

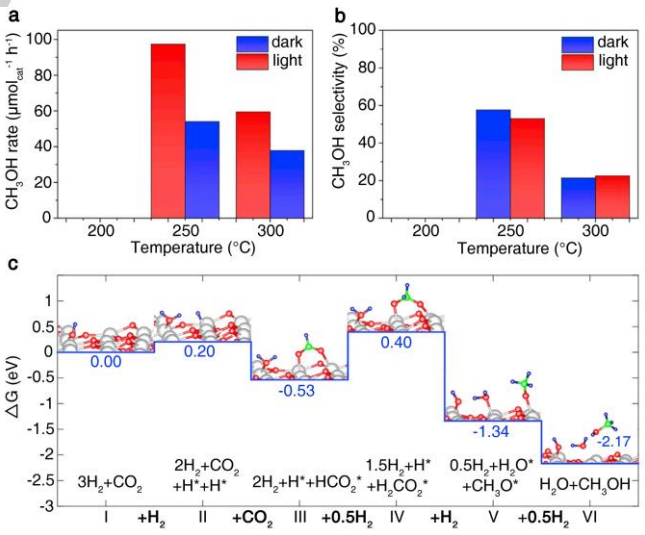

Figure 13. Methanol generation a) rate and b) selectivity over an $In_2O_{3-x}(OH)_y$ nanocrystal superstructure for CO_2 hydrogenation with and without solar irradiation. c) Reaction energy profile from DFT calculations for methanol production *via* CO_2 hydrogenation over $In_2O_{3-x}(OH)_y$. Reproduced with permission.[149] Copyright 2018, Elsevier.

As noted above, plasmonic nanostructures such as Ag and Au nanocrystals can produce photothermal heating from efficient light-to-heat conversion. Unfortunately, these plasmonic metals are inactive for CO_2 hydrogenation to methanol. The combination of plasmonic nanostructures for heating and an active component

for methanol generation represents a fascinating approach to lower reaction temperatures for CO_2 conversion to methanol. Inspired by this, Zeng et al. successfully prepared a Au&Pt@ZIF-8 photocatalyst that was active for CO_2 hydrogenation to methanol at low temperatures.[150] Under light irradiation at 150 °C, the TOF of Au&Pt@ZIF reached as high as 1522 h^{-1}, 13 times higher than that determined for the same material in the dark. The heat generated by the photothermal effect of Au nanocages within the ZIF-8 host enhanced the catalytic activity of the Pt nanocubes.

3.4. Light-driven Higher Hydrocarbon Production

Our group first realized higher hydrocarbon production from light-driven CO_2 hydrogenation over LDH-derived CoFe-based catalysts.[151] A CoFeAl-LDH precursor was reduced at different temperatures (x) in the range 300~700 °C under a H_2 atmosphere. By varying the reduction, a series of CoFe-x catalysts with distinct surface chemistries were obtained, allowing the product selectivity of CO_2 hydrogenation to be progressively tuned from CO to CH_4 and eventually high-value C_{2+} hydrocarbons (**Figure 14a**). Under UV-vis illumination for 2 h, the CoFe-650 catalyst showed a CO_2 conversion of 78.6%, with a C_{2+} selectivity of 35.26% (Figure 14b). Comparative tests showed that photothermal effects caused by catalyst heating under light excitation were responsible for the remarkable catalytic performance (Figure 14c). Comprehensive catalyst characterization studies and DFT calculations revealed that the CoFe-650 catalyst consisted of alumina-supported CoFe alloy NPs, with the formation of the discrete alloy NPs underpinning the high C-C coupling selectivity, leading to the formation of higher hydrocarbons during the CO_2 hydrogenation.

Later, Garcia and co-workers fabricated Na-promoted Co@C NPs which demonstrated excellent catalytic activity for CO_2 hydrogenation to hydrocarbons. Under photothermal conditions, the Na-promoted Co@C catalyst afforded almost 100% selectivity to hydrocarbons (16.5% for C_2, 12.5% for C_3 and 6.5% for ethanol) at >97% CO_2 conversion.[152] Near ambient-pressure X-ray photoelectron spectroscopy (AP-XPS) and in situ Raman spectra analysis showed that light irradiation resulted in the formation of electron rich carbon species on the surface of the Na-Co@C NPs. The mechanism involved CO_2 activation to $CO_2^{\delta-}$, followed by C-O bond dissociation to CO. Further, CO adsorption was stabilized by interaction with the carbon layers on the catalyst surface, enabling the formation of ethanol and C_{2+} hydrocarbons.

Table 2 summarizes recent literature data relating to light-driven CO_2 hydrogenation over various catalysts. Whilst many catalysts are active for solar-driven CO_2 hydrogenation, only a few catalysts (e.g. CoFe alloy NPs and Na-Co@C) allow the production of high value chemicals (e.g. C_{2+} hydrocarbons and methanol). The production of such high value chemicals, which is achieved through judicious balancing of CO_2 dissociation, CH_x-hydrogenation and C-C coupling reactions, is highly desirable and needs more research attention. Moreover, from the viewpoint of sustainable production of solar fuels and artificial photosynthesis, water rather than H_2 is preferable as the hydrogen source. Accordingly, novel methods need to be developed for solar-driven CO_2 reduction with water, for example, the integration of PV-powered electrolytic water splitting with light-driven CO_2 hydrogenation.

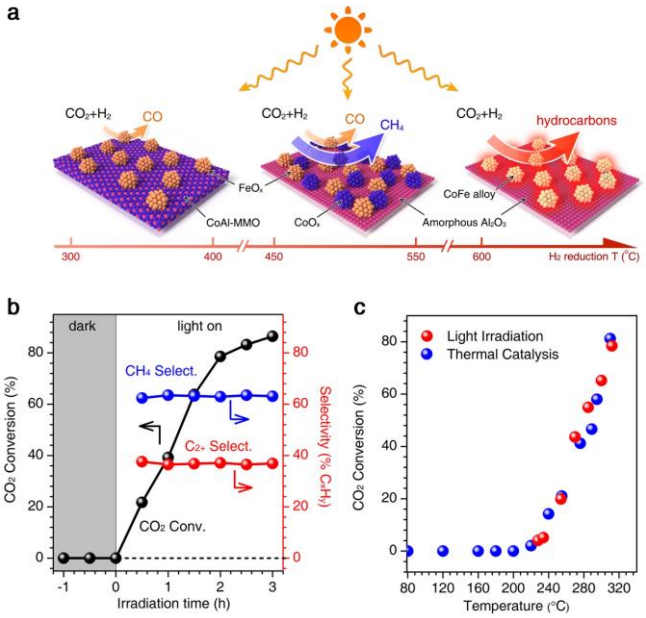

Figure 14. a) Illustration of the different CoFe-*x* catalysts formed by hydrogen reduction of CoFeAl-LDH nanosheets at different temperatures and their catalytic activities for CO_2 hydrogenation. b) Time course of CO_2 conversion and product selectivities for CO_2 hydrogenation over CoFe-650 under UV-Vis irradiation. c) Comparison of CO_2 conversion for CoFe-650 under photothermal heating (UV-Vis irradiation) and direct thermal heating (no UV-Vis irradiation). Reproduced with permission.[151] Copyright 2018, Wiley-VCH.

4. Light-driven Methane Conversion

4.1. Light-driven Methane Oxidation

The photo-oxidation of methane in the presence of oxygen or water is a fascinating approach for the conversion of methane. Kazansky et al. firstly demonstrated that CH_4 could be photochemically oxidized in the presence of O_2 over a TiO_2-based semiconductor photocatalyst under UV irradiation.[153] It was proposed that the hole centers produced on TiO_2, V-doped TiO_2 (V-TiO_2), P-doped TiO_2 (TiO_2) photocatalysts played an important role in activating methane, leading to the formation of methyl radicals. Subsequent research studies found that complete oxidation of methane (COM) to CO_2 and H_2O could be achieved using TiO_2-based semiconductor photocatalysts and uranyl-anchored MCM-41 photocatalysts.[154, 155, 156, 157] Recently, nano-particulate ZnO was found to demonstrate exceptional activity for COM under UV or UV-vis illumination, with the performance superior to commercial TiO_2 (P25) and ZnO (ZnO-C).[158] The COM activity under visible-light illumination could be further enhanced by depositing Ag NPs on the surface of the nano-particulate ZnO, on account of a SPR effect (**Figure 15a**). By examining the wavelength dependence of CH_4 oxidation, it was confirmed that the enhanced reaction rate was due to improved light-absorption properties linked to the Ag NPs (Figure 15b). The quantum yield for CH_4 oxidation was 8% at wavelengths below 400 nm and 0.1% at ~470 nm, indicating the great potential for the utilization of plasmonic in atmospheric methane oxidation. *In situ* EPR and FTIR (Figure 15c, d) studies established that methane photo-oxidation proceeded *via* a two-step process: Firstly, CH_4 reacted with O_2 to produce H_2O and HCHO

Table 2. Performance comparison of different catalysts for CO_2 hydrogenation under light irradiation.

Catalysts	Feed (CO_2:H_2)	Reactor type	Light source	*T* (°C)	Activity[a]	Product Selectivity (%)[b]				Ref.
						CO	CH_4	CH_3OH	C_{2+}	
Ru/RuO_2(3.8%)/TiO_2	1:12	batch	Solar simulator	46	98%	-	100	-	-	[159]
Ru/TiO_2	1:20	flow (CO_2: 1.0 mL min^{-1})	150 W Xe lamp	-	-	-	100	-	-	[139]
$[Zn_3Al(OH)_8]_2[CO_3]$-LDH	~1:9.4	batch	500 W Xe lamp	-	0.16%	94.1	-	5.9	-	[160]
$[Zn_{1.5}Cu_{1.5}Al(OH)_8]_2[CO_3]$-LDH	~1:9.4	batch	500 W Xe lamp	-	0.16%	74.4	-	25.6	-	[160]
$[Zn_{1.5}Cu_{1.5}Ga(OH)_8]_2[CO_3]$-LDH	~1:9.4	batch	500 W Xe lamp	-	0.03%	31.2	-	68.8	-	[160]
$[Zn_3Ga(OH)_8]_2[Cu(OH)_4]$-LDH	~1:9.4	batch	500 W Xe lamp	-	0.04%	30.2	-	69.8	-	[145]
$[Zn_{1.5}Cu_{1.5}Ga(OH)_8]_2[Cu(OH)_4]$-LDH	~1:9.4	batch	500 W Xe lamp	-	0.05%	12.5	-	87.5	-	[145]
Au-ZnO	1:3	batch	532 nm laser	Tunable[c]	Tunable	x (Tunable)	100-x	-	-	[129]
Ru/Al_2O_3	1:4.1	batch	300 W Xe lamp	~360	95.75%	0.78	99.22	-	-	[133]
Rh/Al_2O_3	1:4.1	batch	300 W Xe lamp	~360	96.25%	0.52	99.48	-	-	[133]
Ni/Al_2O_3	1:4.1	batch	300 W Xe lamp	~400	93.25%	0.95	99.05	-	-	[133]
Co/Al_2O_3	1:4.1	batch	300 W Xe lamp	~350	92.58%	0.49	99.51	-	-	[133]
Pd/Al_2O_3	1:4.1	batch	300 W Xe lamp	~350	93.43%	1.36	98.64	-	-	[133]
Pt/Al_2O_3	1:4.1	batch	300 W Xe lamp	~330	60.42%	84.45	15.55	-	-	[133]
Ir/Al_2O_3	1:4.1	batch	300 W Xe lamp	~300	14.94%	36.74	63.25	-	-	[133]
Fe/Al_2O_3	1:4.1	batch	300 W Xe lamp	~310	7.27%	95.96	4.04	-	-	[133]
$Ni/SiO_2{\cdot}Al_2O_3$	1:4.6	batch	Solar simulator	150	94.9%	2.8	97.2	-	-	[161]
NiO	1:4.6	batch	Solar simulator	150	89.8%	-	100	-	-	[161]
Fe_2O_3	1:4.6	batch	Solar simulator	150	51.0%	95.0	4.3	-	0.7	[161]
Au&Pt@ZIF	1:3	batch	Xe lamp	150	1522 h^{-1} (TOF)	-	-	~100	-	[150]
$In_2O_{3-x}(OH)_y$	1:1	batch	1000 W metal halide bulb	150	1.2 μmol g^{-1} h^{-1}	100	-	-	-	[120]
$In_2O_{3-x}(OH)_y$/SiNWs	1:1	batch	300 W Xe lamp	150	22.0 μmol·g^{-1} h^{-1}	100	-	-	-	[121]
Ru/SiNW	1:4	batch	Xe lamp	150	0.99 mmol g^{-1} h^{-1}	-	100	-	-	[162]
ncSi:H	1:1	batch	300 W Xe lamp	150	250 mmol g^{-1} h^{-1}	100	-	-	-	[163]
$Pt/NaTaO_3$	1:1	batch	300 W UV-enhanced Xe lamp	-	139.1 μmol g^{-1} h^{-1}	99.0	1.0	-	-	[164]
$Ru/NaTaO_3$	1:1	batch	300 W UV-enhanced Xe lamp	-	51.8 μmol g^{-1} h^{-1}	4.0	96.0	-	-	[164]
$Pd@Nb_2O_5$	1:1	batch	300 W Xe lamp	-	1.8 mmol g^{-1} h^{-1}	100.0	-	-	-	[165]
Fe@C hybrid	1:1	batch	300 W Xe lamp	-	26.1 mmol g^{-1} h^{-1}	100.0	-	-	-	[166]
Ru@FL-LDH	1:4.1	batch	300 W Xe lamp	~350	96.3% (1 h)	-	99.3	-	-	[167]
Ru@FL-LDH	1:4.1	flow (CO_2: 5.0 mL min^{-1})	300 W Xe lamp	-	277 mmol h^{-1} $mmol_{metal}^{-1}$	-	~100	-	-	[167]
$Ru/TiO_{(2-x)}N_x$	1:4	flow (60mL min^{-1})	300W Xenon lamp, (435nm < λ< 465 nm)	190	15.0 h^{-1} (TOF)	~20.0	~80.0	-	-	[168]
Ru/Al_2O_3	1:3.1	flow (CO_2: 19.5 mL min^{-1})	LEDs	250	24.2 μmol·g^{-1} s^{-1}	<2.0	>98.0	-	-	[143]
Al@Cu_2O	1:1	flow (10 s.c.c.m.)	Fiber laser[d]	~160	0.1 μmol·cm^{-2}·s^{-1}	100.0	-	-	-	[137]
Cu_2O/graphene	1:4	batch	300 W Xe lamp	250	13.93 mmol g^{-1} h^{-1}	trace	99	-	trace	[169]
$In_2O_{3-x}(OH)_y$	1:3	flow (CO_2: 6 mL min^{-1})	130 W Xe lamp	250	183.47 μmol g^{-1} h^{-1}	47	-	53	-	[149]
CoFe alloy/Al_2O_3	1:4	batch	300 W Xe lamp	320	78.6% (2 h)	4.97	59.77	-	35.3	[151]
Na-Co@C	-	batch	1000 W Xe lamp	235	37%	4.8	50.2	-	45	[152]

[a] Catalytic activity including CO_2 conversion (%), turnover frequency (TOF) and CO_2 conversion rate;
[b] The selectivity data have been corrected to product selectivity;
[c] Tunable means that the catalytic reaction can be modified by adjusting the reaction conditions;
[d] Supercontinuum fiber laser (Fianium, 400-850 nm, 4 ps, 80 MHz, 10 W cm^{-2}).

($CH_4 + O_2 \rightarrow HCHO + H_2O$), with the HCHO then reacting with O_2 to form H_2O and CO_2 ($HCHO + O_2 \rightarrow CO_2 + H_2O$). Light-induced surface defects (Zn_o^+ or O_s^-) on ZnO were proposed to play a significant role in methane photo-oxidation process over ZnO-based catalysts, as shown in Figure 15e.

In order to obtain high value oxygen-containing compounds through the POM approach, V, Mo, Bi and W-based photocatalysts have been investigated.[170] For example, formaldehyde was obtained with a selectivity of 76 mol.% on a V_2O_5/SiO_2 photocatalyst.[171] Although TiO_2 and MoO_3 photocatalysts produced only CO_2 *via* CH_4 oxidation, TiO_2-supported MoO_3 can produce both CO and CO_2 under UV irradiation at room temperature, suggesting a synergistic interaction between TiO_2 and MoO_3.[172] MoO_3 on SiO_2 (MoO_3/SiO_2) afforded methanol formation under UV irradiation at 313 K, with the activity able to be further enhanced by addition of Cu^{2+} dopants.[173] Further studies have shown that the addition of certain electron scavengers such as Fe^{3+}, O_2, and H_2O_2 can enhance the POM activity and methanol selectivity of WO_3-based photocatalysts and Bi-based photocatalysts.[174, 175, 176] This enhancement is explained by increased formation of ·OH radicals on the modified catalysts, which then reacted with methane to initiate the production of methanol. Very recently, Tang and co-workers discovered that highly dispersed iron oxide species, including atomically dispersed species anchored on TiO_2 could efficiently and selectively transform methane to methanol under ambient conditions and moderate light irradiation (~1 sun).[177] A photocatalyst with the optimal Fe loading afforded a 15% methane conversion rate with an alcohol selectivity of over 97%. This work identifies a very promising new pathway for the photo-driven oxidation of methane to high value commodity chemicals and feedstocks.

4.2. Light-driven Steam Reforming of Methane

Taylor et al. discovered that methane could react with water to produce methanol and hydrogen over La-doped WO_3 under light irradiation at ~94 °C and atmospheric pressure[178, 179]. Similarly, Villa et al. found that La-doping of mesoporous WO_3 could significantly increase the selectivity and yield of CH_3OH.[175] The enhancement in the performance was mainly attributed to the formation of oxygen vacancies that increased the adsorption of H_2O and modified the surface acid-base properties, resulting in the formation of more ·OH radicals to attack CH_4 on the La-doped WO_3 catalyst. The presence of Ag^+ ions on WO_3 has been shown to enhance the photocatalytic production of methanol by suppressing charge recombination.

Very recently, hot-carrier-induced molecular activation has been explored for methane conversion. Ye and co-workers reported that visible light irradiated TiO_2-supported Rh NPs could greatly enhance methane activation for H_2 production *via* SRM at mild temperatures (**Figure 16**).[180] The apparent activation energy for the reaction decreased by ~50% under light illumination compared with the reaction under dark conditions (Figure 16b). Femtosecond time-resolved infrared spectroscopic studies and DFT calculations confirmed ultrafast separation of hot carriers at the Rh-TiO_2 interface, resulting in the formation of an electron-deficient state of $Rh^{\delta+}$ at the surface for CH_4 activation at low temperatures (Figure 16c, d). Wavelength-dependent activities and kinetic isotope experiments indicated that the photoexcited hot carriers in the Rh NPs played a critical role in the rate-determining step i.e. the cleavage of the C-H bond in CH_4. Deep mechanistic understanding of the Rh-TiO_2 photocatalyst system in light-driven SRM identifies promising new strategies for C-H bond activation through combination of energy-efficient nano-metal photocatalysts and abundant solar light.

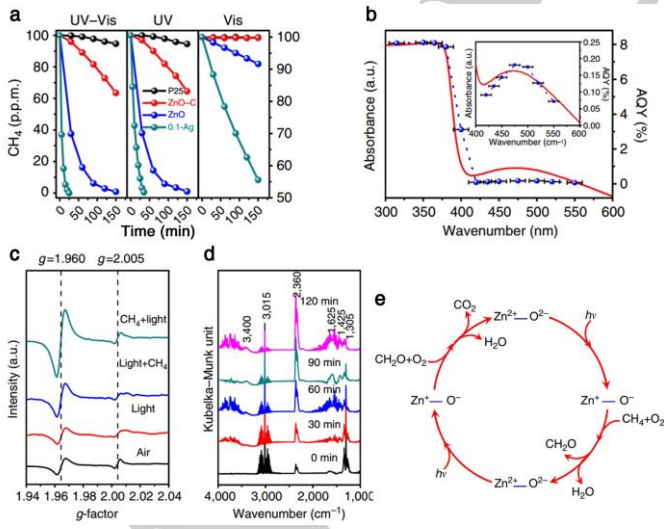

Figure 15. a) Photocatalytic oxidation of CH_4 with light illumination over commercial TiO_2 (P25), commercial ZnO (ZnO-C), ZnO and Ag-ZnO nanocatalysts. b) UV diffuse reflectance spectrum and apparent quantum yield of the 0.1-Ag sample plotted as a function of wavelength of the incident light. c) EPR signals of 0.1-Ag under different conditions. (d) *In situ* IR spectra of CH_4 photocatalytic oxidation collected at different illumination time intervals. e) Schematic for the photocatalytic CH_4 oxidation under ambient conditions. Reproduced with permission.[158] Copyright 2016, Nature Publishing Group.

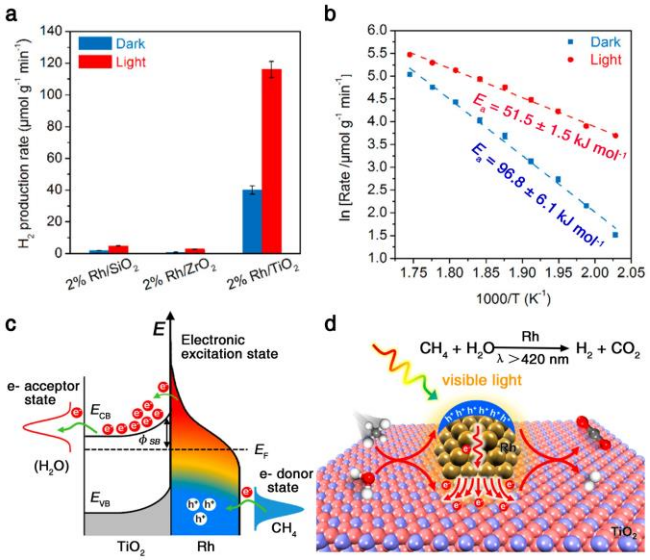

Figure 16. a) Reaction rate of H_2 production on oxide-supported Rh catalysts at 260 °C under dark and light conditions. b) Arrhenius plots for H_2 production under dark and light conditions over Rh/TiO_2 catalysts. c) Schematic of energy transfer from photoexcited hot carriers to adsorbate states. d) Proposed mechanism for SRM reaction on Rh/TiO_2 under visible light illumination. Reproduced with permission.[180] Copyright 2018, American Chemical Society.

4.3. Light-driven Non-Oxidative Coupling of Methane

Pioneering work by Yoshida and co-workers demonstrated that SiO_2-Al_2O_3 showed excellent photocatalytic performance for NOCM around room temperature.[181] Furthermore, they found that pure silica materials previously evacuated at high temperature could promote NOCM at room temperature under light irradiation.[182] The photoactive sites on these pure silica materials were formed through dehydroxylation of surface hydroxyl groups at high temperatures (e.g. 1073 K) before the photoreaction. The catalytic performance of silica could be enhanced by introducing certain metal cations at low loadings, such as Al, Mg and Zr.[183, 184, 185] Highly dispersed titanium oxide and cerium oxide on silica also showed a high activity for NOCM.[186] Ga_2O_3 has very high durability against photoreduction, resulting in the excellent performance for NOCM under UV-light excitation at near room temperature.[187] Benefitting from a higher photo-absorption efficiency and a larger number of the active sites on the surface of the semiconductor photocatalyst, a Ga_2O_3 photocatalyst showed comparable catalytic performance to that of a TiO_2-SiO_2 photocatalyst. In addition to SiO_2-supported photocatalysts, zeolites have good catalytic performance towards NOCM due to their large surface area, uniform pores and abundant and accessible Al-O-Si moieties. The (Zn^+, Zn^{2+})-ZSM-5$^-$ photocatalyst prepared by Chen's group demonstrated excellent catalytic activity and superior selectivity for NOCM to ethane under UV or direct solar irradiation, producing nearly equimolar amounts of ethane and H_2 (**Figure 17**).[188] A catalyst with smaller pores (diameter 0.55 nm) showed excellent selectivity for the formation of ethane (>99.6%) compared to a large pore modified zeolite, suggesting that the shape selectivity of the zeolite framework structure plays a crucial role in NOCM. DFT calculations identified the methane adsorption sites and the mechanism of electron transfer on the active Zn^+ sites. These results confirm that Zn^+ cations in (Zn^+, Zn^{2+})-ZSM-5$^-$ photocatalysts are the active sites for NOCM. This work represented the first example of direct methane conversion driven by light irradiation over zeolites photocatalysts, which has since been extended to other systems such as Ga^{3+}-modified ETS-10 for the photoactivation of the C-H bond of methane.[189, 190]

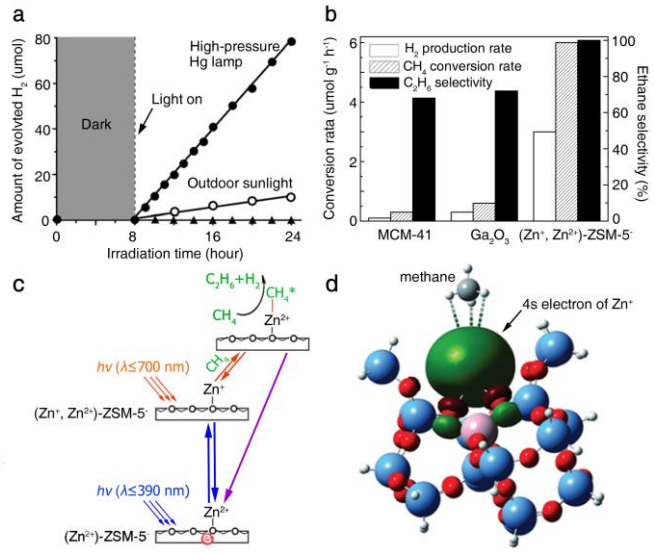

Figure 17. a) Photocatalytic hydrogen evolution *via* the NOCM reaction catalyzed by (Zn^+, Zn^{2+})-ZSM-5$^-$ catalyst. b) Methane and hydrogen production rates, and ethane selectivity for the NOCM reaction catalyzed by different photocatalysts. c) Schematic energy diagram for the processes involved in the photocatalytic NOCM reaction over Zn-ZSM-5 catalyst. d) The optimized geometry of methane on Zn^+ active sites. Reproduced with permission.[188] Copyright 2011, Wiley-VCH.

In addition, the direct conversion of CH_4 to synthetically useful compounds such as olefins and aromatics is now attracting much attention. Si-doped GaN nanowire semiconductor photocatalysts with a 97% rationally constructed m-plane synthesized by Li's group could directly convert methane into benzene and hydrogen under ultraviolet light excitation at room temperature.[191] The introduction of Si-donor or Mg-acceptor dopants into GaN further enhanced the photocatalytic performance.

4.4. Light-driven Dry Reforming of Methane

Metallic Rh is an outstanding catalyst for DRM in conventional thermal catalysis. Ye and co-workers discovered that Au NPs could serve as a plasmonic promoter and efficiently accelerate the DRM reaction over a Rh/SBA-15 catalyst upon visible irradiation.[192] Since Au is generally regarded as being inactive in DRM reaction, the photo-enhanced activity could be directly attributed to the excitation of the Au NPs by visible light. As depicted in **Figure 18a-d**, light irradiation at 490-550 nm (directly under the Au LSPR band) greatly enhanced the catalytic activity for DRM. Electromagnetic field simulations results allowed rationalization of the catalytic activities. Among Rh/SBA-15, Au/SBA-15, and Rh-Au/SBA-15 catalysts, the latter showed the highest localized electric-field enhancement due to the interparticle coupling between the Au NPs and the Rh NPs, favoring the photoactivation of CH_4 and CO_2 *via* a plasmonic dipole (Figure 18e-g). Similarly, Au/Rh NPs modified titanate nanotubes,[193] Pd-Au/Al_2O_3[194], Pt-Au/SiO_2[195], Pt/CeO_2[196] all exhibited excellent photocatalytic activity for DRM *via* LSPR-assistance effects. The introduction of a plasmonic promoter thus provides a viable approach for introducing an extra photo activation mechanism into tradition thermally-driven catalyst systems.

Ni-based catalysts have attracted considerable attention for thermal-catalytic DRM due to their low cost and relatively high catalytic activity.[197] However, the Ni-based catalysts suffer from rapid deactivation during DRM due to carbon deposition on the Ni surface, which has limited their utilization in industry. Thermodynamic analysis showed that carbon deposition is thermodynamically favorable during DRM at temperatures below 1000 °C[198], originating mainly from the decomposition of CH_4 and the disproportionation of CO. Based on this information, Li's group developed novel silica-cluster-modified Ni nanocrystals supported on mesoporous silica (denoted as SCM-Ni/SiO_2), which completely suppressed carbon deposition during DRM, thereby affording a DRM catalyst with excellent activity and durability.[199] Subsequently, they reported efficient DRM in a continuous flow reactor under solar light irradiation,[199] with very high production rates of H_2 (17.1 mmol min^{-1} g^{-1}) and CO (19.9 mmol min^{-1} g^{-1}). The solar-to-fuel efficiency of the SCM-Ni/SiO_2 catalyst reached as high as 12.5%.

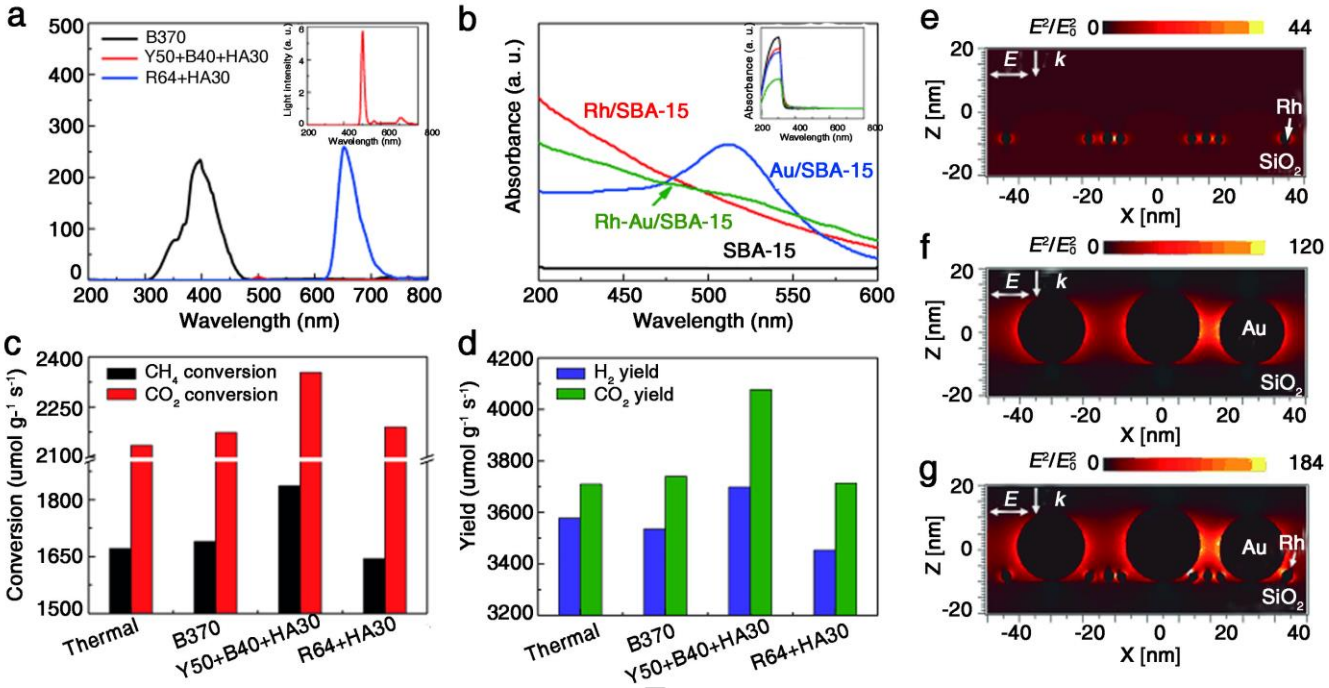

Figure 18. a) Light outputs obtained using different filter sets (the inset shows the wavelength of Y50+B440+HA30). b) UV-vis spectra of different catalysts (the inset shows the spectra between 200-800 nm). c) CH_4 and CO_2 conversions (d) and H_2 and CO yields without or with light irradiation in different wavelength ranges. e-g) Cross-sectional views of the electromagnetic field distribution and enhancement simulated using the FDTD method. e) Rh/SBA-15, f) Au/SBA-15, and g) Rh-Au/SBA-15. Reproduced with permission.[192] Copyright 2015, Wiley-VCH.

5. Light-driven C-C coupling of methanol

Methanol can be converted into valuable chemicals through C-C coupling reactions, typically involving the activation of the O-H or C-O bond. As a multi-carbon compound, ethylene glycol (EG) is widely used in the manufacture of polyesters, especially poly-(ethylene terephthalate) (PET).[200] Unfortunately, the production of EG *via* a direct C-C coupling of methanol is hard *via* traditional thermal catalysis due to the thermodynamic barriers. Solar-driven photocatalysis is therefore a promising alternative strategy to realize C-C coupling under mild conditions. Wang et al. reported visible-light-driven dehydrogenative coupling of methanol to EG with 90% selectivity and high efficiency over a MoS_2 nano foam-modified CdS nanorod catalyst (**Figure 19a**).[201] Experimental results revealed that the MoS_2 nanofoam served as a co-catalyst and subsequently accelerated the photocatalytic activity for EG formation by providing H_2-evolution active sites and also enhancing the transfer of photogenerated electrons and holes (Figure 19b). Upon light irradiation, the rate of formation of EG and H_2 on the 5.0 wt.% MoS_2 foam/CdS were 11 mmol g_{cat}^{-1} h^{-1} and 12 mmol g_{cat}^{-1} h^{-1}, respectively. These rates were 24 and 16 times higher than those for the bare CdS nanorod photocatalyst. Mechanistic studies including *in-situ* electron spin resonance spectra and DFT calculations (Figure 19c) revealed preferential activation of a C-H bond in methanol by photoexcited holes on CdS *via* a concerted proton-electron transfer mechanism to form a hydroxymethyl radical ($\cdot CH_2OH$). This radical could then readily detach from the catalyst surface to participate in C-C coupling reactions. This work offers a novel approach for EG synthesis and suggests a new synthetic strategy for chemical reactions involving preferential C-H bond activation.

Ma et al. realized hydrogen evolution from methanol at low temperatures *via* methanol reforming.[82] It is therefore anticipated that in the coming years, light-driven methanol conversion devices might be coupled with H_2 fuel cells for automotive applications, allowing the advantages of methanol as an energy/hydrogen carrier and H_2 as a fuel to be fully exploited. Another C1 molecule that can be derived from methanol, formaldehyde (HCHO), can be also utilized as a raw material for C-C coupling reactions and the production of higher-valuable chemicals under light irradiation.[202, 203]

6. Conclusions and Perspectives

Catalytic C1 chemistry is fascinating from both an academic and industrial perspective. Light-induced C1 transformations offer a cleaner pathway for the production of fuels and commodity chemicals by harnessing abundant solar energy. In this review, we highlighted recent developments in the conversion of simple C1 molecules, including CO, CO_2, CH_4 and CH_3OH, to valuable products, placing special emphasis on the catalyst design and fundamental reaction mechanisms. Enormous recent progress has been made in the field of light-driven C1 chemistry, though catalytic activities are still not high sufficient to demand serious consideration in practical applications. Thus, to narrow the gap between today's knowledge and industry performance requirements, the following issues need to be addressed:

(1) FTs is the core of industrial C1 chemistry, through which simple C1 molecules are transformed into value-added

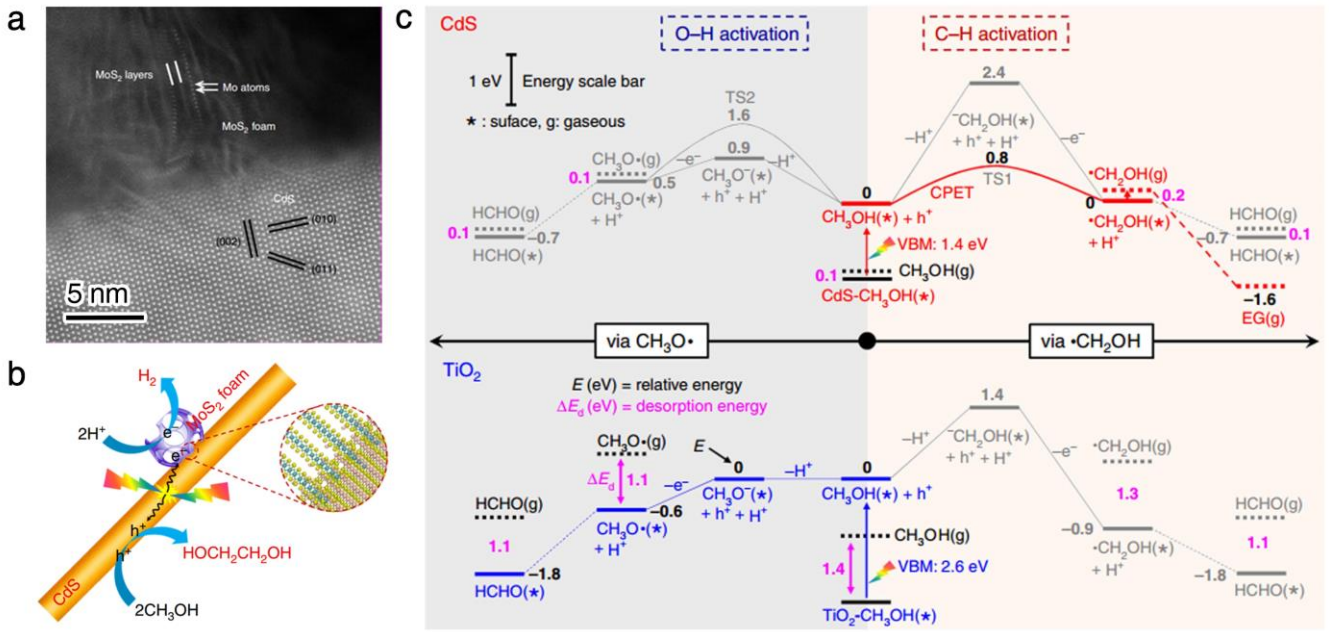

Figure 19. Visible light-driven C-H activation and C-C coupling of methanol into EG over a MoS_2 foam/CdS catalyst. a) High-angle annular dark field-STEM image of MoS_2 foam/CdS. b) Schematic illustration of photocatalytic synthesis of EG and H_2 from CH_3OH over MoS_2 foam/CdS catalysts. c) Reaction energy profiles *via* $\cdot CH_2OH$ and $CH_3O\cdot$ on CdS (100) and rutile TiO_2 (110). Reproduced with permission.[201] Copyright 2018, Nature Publishing Group

commodity chemicals. Very few reports to date actually focus on light-driven FTs. Thus, intensive research effort should be directed in the future towards solar-drive FTs catalyst design and underpinning reaction mechanisms. The few studies that have been reported reveal unique pathways for CO activation and conversion under light irradiation. For example, photocatalytic activities and product selectivities are able to be tuned simply by changing the light wavelength and light intensity, thereby allowing the production of desired fuels and commodity chemicals.

(2) Light-driven CO_2 hydrogenation for the production of methane has already been demonstrated with high CO_2 conversions and CH_4 selectivities (>95%), with CH_4 production rates >1 mmol g_{cat}^{-1} h^{-1} achieved over supported Ru, Rh and Ni NPs. By obtaining H_2 from renewable resources (e.g. H_2O splitting using electrolyzers and renewable electricity), sustainable CO_2 conversion to CH_4 should be viable in the near future. Taking inspiration from this, combining a water-splitting photocatalyst and a CO_2-active photocatalyst into one system would appear a prudent strategy for solar-driven CO_2 hydrogenation to CH_4. However, the production of C_{2+} hydrocarbons *via* light-driven CO_2 hydrogenation is still extremely challenging. Potentially by integrating the RWGS and FT processes ($CO_2 + H_2 \rightarrow CO$, then $CO + H_2 \rightarrow$ hydrocarbons) or a methanol-mediated process ($CO_2 + H_2 \rightarrow CH_3OH$, then $CH_3OH \rightarrow$ hydrocarbons), the generation of value-added C_{2+} hydrocarbons at meaningful rates might become possible.

(3) Regarding light-driven CH_4 conversion, typically additional heat input is needed to drive the reaction at meaningful rates. Thus, next generation photocatalysts should be cheap, active and stable against oxidation at reaction temperatures, as well as resistant to coking, sintering, poisoning and light-induced corrosion. Bimetallic and multi-metallic catalysts allow manipulation of the surface electronic properties of catalysts, benefitting both catalyst reactivity, selectivity and stability. Further, the catalyst support plays a key role in ensuring a high active phase dispersion, requiring good understanding of the metal-support interaction. Additionally, the construction of 2D nanomaterials with abundant coordinatively unsaturated metal sites can be highly beneficial for the light-driven processes such as NOCM, motivating research into structure-activity relationships for both thermal and photo-driven catalyst systems.

(4) Heterogeneous catalyzed C1 conversions typically require high temperatures and pressures to achieve C1 molecule activation and conversion, with conversion rates and selectivity typically controlled by the thermodynamics or kinetics. Such extreme operating conditions can cause catalyst overheating and sintering, thereby reducing catalyst lifetimes. In comparison, processes utilizing light such as photocatalysis (electron-hole excitation), photothermal catalysis (local heating) and plasmonic catalysis(dipole effect, etc.) can be run at lower temperatures and pressures, thereby avoiding catalyst deactivation through sintering and thereby extending catalyst lifetimes. Moreover, the product selectivity can be tuned by changing the light intensity or wavelength.

(5) Light irradiation under appropriate conditions enhances C1 conversion on many supported metal catalysts (especially Ru, Rh or Ni). In many cases, both photocatalytic and photothermal processes occur simultaneously on the catalyst surface, playing a role in both reactant activation and conversion processes. In order to optimize catalyst design, it is imperative to be able to distinguish the contributions of light-driven and heat-driven processes on the product distribution. Identifying possible reaction pathways and the rate-determining elementary step, pinpointing the role of electrons and holes, understanding photothermal phenomena, and other relevant aspects needs studied deeply and systematically to allow meaningful conclusions to be drawn regarding a particular light-driven reaction.

(6) To date, Group IB metals (Au, Ag and Cu) have been used widely for light-driven CO_2 and CH_4 conversions. A shift towards

other plasmonic nanometals for C1 molecule activation and conversion is highly desirable. In this context, Group VIII plasmonic nanometals are particularly deserving of consideration owing to their excellent catalytic activity in conventional thermal catalysis. In principle, any C1 process involving thermal catalysis should be able to be driven by a light-assisted process (*via* LSPR-mediated catalysis) at a lower reaction temperature. However, the switch to a light-assisted process will likely require a radical rethink of catalyst design and reactor configuration to allow for full catalyst bed irradiation with light. Recent literature suggests that the combination of plasmonic nanometals and conventional thermal-catalytic metals is likely to be the most effective strategy for achieving industry-relevant CO_2 conversion rates.

(7) Detailed catalyst characterization underpins the establishment of structure-performance relationships. In order to achieve this goal, more advanced *in situ* techniques are needed, to complement existing techniques such as *in-situ* XAFS, *in-situ* XPS, *in-situ* XRD, *in-situ* transient absorption spectroscopy and *in-situ* FTIR spectroscopy which are now becoming mainstream in catalysis and photocatalysis research. It is vital to be able to study catalysts before, during and after catalytic and photocatalytic reactions, thereby allowing changes in catalyst composition and structure during reaction to be correlated with activity, selectivity and stability. Such techniques and information garnered through their application guide the rational design of improved catalysts. Ground state DFT calculations on thermal catalysts are now routine and offer great insights for explaining and predicting C1 conversion selectivities. However, excited state DFT calculations which are highly relevant to the photocatalytic reactions remain in their infancy. Excited state DFT calculations are expected to be able to provide direct information about of the roles of photons, electrons and holes in the photocatalytic processes, critical information to the understanding the reaction mechanisms.

(8) In most reports of light-driven C1 chemistry, the catalytic experiments have been conducted in the gas phase using batch reactors with small volumes (~100 mL) over several hours. In such batch reactor systems, isotopic experiments are advisable to trace the carbon source. Most importantly, transiting from a batch reactor to a flow-type-photo-reactor is essential from an industrial viewpoint. Indeed, there are a number of advantages in switching to flow-type-photo-reactors, such as higher conversions and the avoidance of local overheating and catalyst sintering. For hydrogenation reactions, flow-type-photo-reactors are highly desirable to avoid the over hydrogenation of olefin products to alkanes (a limitation of batch reactors). Thus, the testing of light-driven C1 conversion catalysts under both batch and flow conditions is highly recommended. Furthermore, in the evaluating catalysts for light-driven C1 chemistry, stability tests reported are typically less than 10 h. Stability tests over much longer time periods (weeks to months) are necessary for industry purposes.

(9) From the point of scale-up, feasibility studies encompassing lab prototypes and industrial scale pilot plants are critical on the path to commercialization. This requires chemists and engineers working closely and synergistically to optimize catalyst performance at each process stage and scale, placing particular emphasis of photoreactor design as well as mass, light and heat flow through the reactor. The economics of any C1 conversion process as a function of process scale also needs careful consideration.

In summary, light-driven C1 chemistry is currently attracting a lot of attention from the scientific community, with interest and research activity in this field expected to grow enormously over the next few decades. Some promising discoveries have recently been made relating to the understanding of light-driven C1 reactions, which inspire confidence that in the not-too-distant future light-driven processes may replace some conventional thermal catalytic reactions in the chemical industry**.**

Acknowledgements

The authors are grateful for the financial support from the National Key Projects for Fundamental Research and Development of China (2018YFB1502002, 2016YFB0600901, 2017YFA0206904, 2017YFA0206900), the National Natural Science Foundation of China (51825205, U1662118, 51772305, 51572270, 21871279, 21802154), the Beijing Natural Science Foundation (2191002, 2194089, 2182078), the Strategic Priority Research Program of the Chinese Academy of Sciences (XDB17000000), the Beijing Municipal Science and Technology Project (Z181100005118007), the Royal Society-Newton Advanced Fellowship (NA170422), the K. C. Wong Education Foundation and the International Partnership Program of Chinese Academy of Sciences (GJHZ1819). G. Chen thanks the funding from China Scholarship Council. G. I.N. Waterhouse acknowledges funding support from the University of Auckland Faculty Research Development Fund, the Energy Education Trust of New Zealand and the MacDiarmid Institute for Advanced Materials and Nanotechnology.

Keywords: solar fuels • C1 chemistry • photocatalysis • Fischer-Tropsch synthesis • CO_2 hydrogenation

References

[1] R. Schlögl, *ChemSusChem* **2010**, *3*, 209.
[2] G. A. Olah, *Angew. Chem., Int. Ed.* **2013**, *52*, 104.
[3] N. L. Panwar, S. C. Kaushik, S. Kothari, *Rene. Sust. Energ. Rev.* **2011**, *15*, 1513.
[4] S. Chu, Y. Cui, N. Liu, *Nat. Mater.* **2016**, *16*, 16.
[5] S. Wang, I. Agirrezabal-Telleria, A. Bhan, D. Simonetti, K. Takanabe, E. Iglesia, *Faraday Discuss.* **2017**, *197*, 9.
[6] Y. Zhao, G. I. N. Waterhouse, G. Chen, X. Xiong, L.-Z. Wu, C.-H. Tung, T. Zhang, *Chem. Soc. Rev.* **2018**, *DOI: 10.1039/C8CS00607E*.
[7] G. A. Olah, Á. Molnár, *Hydrocarbon chemistry*, John Wiley & Sons, **2003**.
[8] Q. Yi, W. Li, J. Feng, K. Xie, *Chem. Soc. Rev.* **2015**, *44*, 5409.
[9] C. B. Roberts, N. O. Elbashir, *Fuel Sci. Technol.* **2003**, *83*, 1.
[10] C. Mesters, *Annu. Rev. Chem. Biomol. Eng.* **2016**, *7*, 223.
[11] Q. Zhang, J. Kang, Y. Wang, *ChemCatChem* **2010**, *2*, 1030.
[12] S. Saeidi, N. A. S. Amin, M. R. Rahimpour, *J. CO_2 Util.* **2014**, *5*, 66.
[13] J. H. Lunsford, *Catal. Today* **2000**, *63*, 165.
[14] J. F. Haw, W. Song, D. M. Marcus, J. B. Nicholas, *Acc. Chem. Res.* **2003**, *36*, 317.
[15] M. E. Dry, *Catal. Today* **2002**, *71*, 227.
[16] V. R. Calderone, N. R. Shiju, D. Curulla-Ferré, S. Chambrey, A. Khodakov, A. Rose, J. Thiessen, A. Jess, G. Rothenberg, *Angew. Chem., Int. Ed.* **2013**, *52*, 4397.
[17] W. Gao, Q. Zhu, D. Ma, *Chinese J. Chem.* **2018**, *36*, 798.
[18] H. M. Torres Galvis, K. P. de Jong, *ACS Catal.* **2013**, *3*, 2130.
[19] G. P. Van Der Laan, A. Beenackers, *Catal. Rev. Sci. Eng.* **1999**, *41*, 255.
[20] B. C. Enger, A. Holmen, *Catal. Rev. Sci. Eng.* **2012**, *54*, 437.
[21] A. Y. Khodakov, W. Chu, P. Fongarland, *Chem. Rev.* **2007**, *107*, 1692.
[22] S. Li, S. Krishnamoorthy, A. Li, G. D. Meitzner, E. Iglesia, *J. Catal.* **2002**, *206*, 202.
[23] J. P. d. Breejen, J. R. A. Sietsma, H. Friedrich, J. H. Bitter, K. P. d. Jong, *J. Catal.* **2010**, *270*, 146.

[24] H. M. Torres Galvis, J. H. Bitter, C. B. Khare, M. Ruitenbeek, A. I. Dugulan, K. P. de Jong, *Science* **2012**, *335*, 835.
[25] J. Gaube, H. F. Klein, *Appl. Catal. A: Gen.* **2008**, *350*, 126.
[26] P. Zhai, C. Xu, R. Gao, X. Liu, M. Li, W. Li, X. Fu, C. Jia, J. Xie, M. Zhao, X. Wang, Y. W. Li, Q. Zhang, X. D. Wen, D. Ma, *Angew. Chem., Int. Ed.* **2016**, *55*, 9902.
[27] R. Guettel, U. Kunz, T. Turek, *Chem. Eng. Technol.* **2008**, *31*, 746.
[28] H. Jahangiri, J. Bennett, P. Mahjoubi, K. Wilson, S. Gu, *Catal. Sci. Technol.* **2014**, *4*, 2210.
[29] Y. Zhai, D. Pierre, R. Si, W. Deng, P. Ferrin, A. U. Nilekar, G. Peng, J. A. Herron, D. C. Bell, H. Saltsburg, M. Mavrikakis, M. Flytzani-Stephanopoulos, *Science* **2010**, *329*, 1633.
[30] M. Zhu, I. E. Wachs, *ACS Catal.* **2016**, *6*, 722.
[31] C. Rhodes, G. J. Hutchings, *Phys. Chem. Chen. Phys.* **2003**, *5*, 2719.
[32] A. Khan, P. Chen, P. Boolchand, P. G. Smirniotis, *J. Catal.* **2008**, *253*, 91.
[33] J. Y. Lee, D.-W. Lee, Y.-K. Hong, K.-Y. Lee, *Int. J. Hydrog.Energy* **2011**, *36*, 8173.
[34] R. Radhakrishnan, R. R. Willigan, Z. Dardas, T. H. Vanderspurt, *AIChE J.* **2006**, *52*, 1888.
[35] Q. Fu, H. Saltsburg, M. Flytzani-Stephanopoulos, *Science* **2003**, *301*, 935.
[36] J. A. Rodriguez, S. Ma, P. Liu, J. Hrbek, J. Evans, M. Pérez, *Science* **2007**, *318*, 1757.
[37] V. Scott, S. Gilfillan, N. Markusson, H. Chalmers, R. S. Haszeldine, *Nat. Clim. Change* **2013**, *3*, 105.
[38] S. Lin, C. S. Diercks, Y.-B. Zhang, N. Kornienko, E. M. Nichols, Y. Zhao, A. R. Paris, D. Kim, P. Yang, O. M. Yaghi, *Science* **2015**, *349*, 1208.
[39] S. Gao, Y. Lin, X. Jiao, Y. Sun, Q. Luo, W. Zhang, D. Li, J. Yang, Y. Xie, *Nature* **2016**, *529*, 68.
[40] R. W. Dorner, D. R. Hardy, F. W. Williams, H. D. Willauer, *Energy Environ. Sci.* **2010**, *3*, 884.
[41] W. Wang, S. Wang, X. Ma, J. Gong, *Chem. Soc. Rev.* **2011**, *40*, 3703.
[42] T. Sakakura, J.-C. Choi, H. Yasuda, *Chem. Rev.* **2007**, *107*, 2365.
[43] M. Mikkelsen, M. Jorgensen, F. C. Krebs, *Energy Environ. Sci.* **2010**, *3*, 43.
[44] F. S. Stone, D. Waller, *Top. Catal.* **2003**, *22*, 305.
[45] C.-S. Chen, W.-H. Cheng, S.-S. Lin, *Chem. Commun.* **2001**, 1770.
[46] K. P. Brooks, J. Hu, H. Zhu, R. J. Kee, *Chem. Eng. Sci.* **2007**, *62*, 1161.
[47] P. Frontera, A. Macario, M. Ferraro, P. Antonucci, *Catalysts* **2017**, *7*, 59.
[48] K. Fujimoto, T. Shikada, *Appl. Catal.* **1987**, *31*, 13.
[49] P. S. Prasad, J. W. Bae, K.-W. Jun, K.-W. Lee, *Catal. Surv. Asia.* **2008**, *12*, 170.
[50] M. Behrens, F. Studt, I. Kasatkin, S. Kühl, M. Hävecker, F. Abild-Pedersen, S. Zander, F. Girgsdies, P. Kurr, B.-L. Kniep, M. Tovar, R. W. Fischer, J. K. Nørskov, R. Schlögl, *Science* **2012**, *336*, 893.
[51] J. Graciani, K. Mudiyanselage, F. Xu, A. E. Baber, J. Evans, S. D. Senanayake, D. J. Stacchiola, P. Liu, J. Hrbek, J. F. Sanz, J. A. Rodriguez, *Science* **2014**, *345*, 546.
[52] F. Studt, I. Sharafutdinov, F. Abild-Pedersen, C. F. Elkjær, J. S. Hummelshøj, S. Dahl, I. Chorkendorff, J. K. Nørskov, *Nat. Chem.* **2014**, *6*, 320.
[53] E. M. Fiordaliso, I. Sharafutdinov, H. W. P. Carvalho, J.-D. Grunwaldt, T. W. Hansen, I. Chorkendorff, J. B. Wagner, C. D. Damsgaard, *ACS Catal.* **2015**, *5*, 5827.
[54] P. G. Jessop, T. Ikariya, R. Noyori, *Chem. Rev.* **1995**, *95*, 259.
[55] P. G. Jessop, F. Joó, C.-C. Tai, *Coordin. Chem. Rev.* **2004**, *248*, 2425.
[56] P. Tang, Q. Zhu, Z. Wu, D. Ma, *Energy Environ. Sci.* **2014**, *7*, 2580.
[57] M. Belgued, P. Pareja, A. Amariglio, H. Amariglio, *Nature* **1991**, *352*, 789.
[58] L. Wang, L. Tao, M. Xie, G. Xu, J. Huang, Y. Xu, *Catal. Lett.* **1993**, *21*, 35.
[59] Y. Xu, X. Bao, L. Lin, *J. Catal.* **2003**, *216*, 386.
[60] X. Guo, G. Fang, G. Li, H. Ma, H. Fan, L. Yu, C. Ma, X. Wu, D. Deng, M. Wei, D. Tan, R. Si, S. Zhang, J. Li, L. Sun, Z. Tang, X. Pan, X. Bao, *Science* **2014**, *344*, 616.
[61] I. Yamanaka, M. Soma, K. Oisuka, *J. Chem. Soc. Chem. Commun.* **1995**, *21*, 2235.
[62] H. Liu, C. Song, L. Zhang, J. Zhang, H. Wang, D. P. Wilkinson, *J. Power Sources* **2006**, *155*, 95.
[63] R. A. Periana, D. J. Taube, S. Gamble, H. Taube, T. Satoh, H. Fujii, *Science* **1998**, *280*, 560.
[64] T. Zimmermann, M. Soorholtz, M. Bilke, F. Schüth, *J. Am. Chem. Soc.* **2016**, *138*, 12395.
[65] R. A. Periana, D. J. Taube, E. R. Evitt, D. G. Löffler, P. R. Wentrcek, G. Voss, T. Masuda, *Science* **1993**, *259*, 340.
[66] M. Muehlhofer, T. Strassner, W. A. Herrmann, *Angew. Chem., Int. Ed.* **2002**, *41*, 1745.
[67] W. Huang, S. Zhang, Y. Tang, Y. Li, L. Nguyen, Y. Li, J. Shan, D. Xiao, R. Gagne, A. I. Frenkel, F. Tao, *Angew. Chem., Int. Ed.* **2016**, *55*, 13441.
[68] V. L. Sushkevich, D. Palagin, M. Ranocchiari, J. A. van Bokhoven, *Science* **2017**, *356*, 523.
[69] V. I. Sobolev, K. A. Dubkov, O. V. Panna, G. I. Panov, *Catal. Today* **1995**, *24*, 251.
[70] C. Hammond, M. M. Forde, M. H. Ab Rahim, A. Thetford, Q. He, R. L. Jenkins, N. Dimitratos, J. A. Lopez-Sanchez, N. F. Dummer, D. M. Murphy, A. F. Carley, S. H. Taylor, D. J. Willock, E. E. Stangland, J. Kang, H. Hagen, C. J. Kiely, G. J. Hutchings, *Angew. Chem., Int. Ed.* **2012**, *51*, 5129.
[71] C. Hammond, N. Dimitratos, J. A. Lopez-Sanchez, R. L. Jenkins, G. Whiting, S. A. Kondrat, M. H. ab Rahim, M. M. Forde, A. Thetford, H. Hagen, E. E. Stangland, J. M. Moulijn, S. H. Taylor, D. J. Willock, G. J. Hutchings, *ACS Catal.* **2013**, *3*, 1835.
[72] M. H. Groothaert, P. J. Smeets, B. F. Sels, P. A. Jacobs, R. A. Schoonheydt, *J. Am. Chem. Soc.* **2005**, *127*, 1394.
[73] S. Grundner, M. A. C. Markovits, G. Li, M. Tromp, E. A. Pidko, E. J. M. Hensen, A. Jentys, M. Sanchez-Sanchez, J. A. Lercher, *Nat. Commun.* **2015**, *6*, 7546.
[74] N. Agarwal, S. J. Freakley, R. U. McVicker, S. M. Althahban, N. Dimitratos, Q. He, D. J. Morgan, R. L. Jenkins, D. J. Willock, S. H. Taylor, C. J. Kiely, G. J. Hutchings, *Science* **2017**, *358*, 223.
[75] X. Cui, H. Li, Y. Wang, Y. Hu, L. Hua, H. Li, X. Han, Q. Liu, F. Yang, L. He, X. Chen, Q. Li, J. Xiao, D. Deng, X. Bao, *Chem* **2018**, *4*, 1902.
[76] A. P. E. York, T. Xiao, M. L. H. Green, *Top. Catal.* **2003**, *22*, 345.
[77] D. Li, Y. Nakagawa, K. Tomishige, *Appl. Catal. A: Gen.* **2011**, *408*, 1.
[78] H. Ceri, C. Sabrina, H. Ive, *ChemSusChem* **2012**, *5*, 1668.
[79] Q. Zhu, S. L. Wegener, C. Xie, O. Uche, M. Neurock, T. J. Marks, *Nat. Chem.* **2012**, *5*, 104.
[80] R. D. Cortright, R. R. Davda, J. A. Dumesic, *Nature* **2002**, *418*, 964.
[81] D. R. Palo, R. A. Dagle, J. D. Holladay, *Chem. Rev.* **2007**, *107*, 3992.
[82] L. Lin, W. Zhou, R. Gao, S. Yao, X. Zhang, W. Xu, S. Zheng, Z. Jiang, Q. Yu, Y.-W. Li, C. Shi, X.-D. Wen, D. Ma, *Nature* **2017**, *544*, 80.
[83] M. Nielsen, E. Alberico, W. Baumann, H.-J. Drexler, H. Junge, S. Gladiali, M. Beller, *Nature* **2013**, *495*, 85.
[84] C. D. Chang, A. J. Silvestri, *J. Catal.* **1977**, *47*, 249.
[85] P. Tian, Y. Wei, M. Ye, Z. Liu, *ACS Catal.* **2015**, *5*, 1922.
[86] B. P. C. Hereijgers, F. Bleken, M. H. Nilsen, S. Svelle, K.-P. Lillerud, M. Bjørgen, B. M. Weckhuysen, U. Olsbye, *J. Catal.* **2009**, *264*, 77.
[87] U. Olsbye, S. Svelle, M. Bjørgen, P. Beato, T. V. W. Janssens, F. Joensen, S. Bordiga, K. P. Lillerud, *Angew. Chem., Int. Ed.* **2012**, *51*, 5810.
[88] C. Li, C. Paris, J. Martínez-Triguero, M. Boronat, M. Moliner, A. Corma, *Nat. Catal.* **2018**, *1*, 547.
[89] S. Ilias, A. Bhan, *ACS Catal.* **2013**, *3*, 18.
[90] J. Q. Chen, A. Bozzano, B. Glover, T. Fuglerud, S. Kvisle, *Catal. Today* **2005**, *106*, 103.
[91] F. J. Keil, *Microporous Mesoporous Mater.* **1999**, *29*, 49.
[92] I. M. Dahl, S. Kolboe, *Catal. Lett.* **1993**, *20*, 329.
[93] C. F. Shih, T. Zhang, J. Li, C. Bai, *Joule* **2018**, *2*, 1925.
[94] S. N. Habisreutinger, L. Schmidt-Mende, J. K. Stolarczyk, *Angew. Chem., Int. Ed.* **2013**, *52*, 7372.
[95] Y. Ma, X. Wang, Y. Jia, X. Chen, H. Han, C. Li, *Chem. Rev.* **2014**, *114*, 9987.
[96] X. Chang, T. Wang, J. Gong, *Energy Environ. Sci.* **2016**, *9*, 2177.
[97] S. Chu, P. Ou, P. Ghamari, S. Vanka, B. Zhou, I. Shih, J. Song, Z. Mi, *J. Am. Chem. Soc.* **2018**, *140*, 7869.
[98] L. Zhang, Z.-J. Zhao, T. Wang, J. Gong, *Chem. Soc. Rev.* **2018**, *47*, 5423.
[99] X.-N. Guo, Z.-F. Jiao, G.-Q. Jin, X.-Y. Guo, *ACS Catal.* **2015**, *5*, 3836.
[100] F. Sastre, A. Corma, H. García, *Angew. Chem., Int. Ed.* **2013**, *52*, 12983.
[101] Y. Zhao, B. Zhao, J. Liu, G. Chen, R. Gao, S. Yao, M. Li, Q. Zhang, L. Gu, J. Xie, X. Wen, L.-Z. Wu, C.-H. Tung, D. Ma, T. Zhang, *Angew. Chem., Int. Ed.* **2016**, *55*, 4215.
[102] Z. Li, J. Liu, Y. Zhao, G. I. N. Waterhouse, G. Chen, R. Shi, X. Zhang, X. Liu, Y. Wei, X.-D. Wen, L.-Z. Wu, C.-H. Tung, T. Zhang, *Adv. Mater.* **2018**, *30*, 1800527.
[103] Y. Zhao, Z. Li, M. Li, J. Liu, X. Liu, G. I. N. Waterhouse, Y. Wang, J. Zhao, W. Gao, Z. Zhang, R. Long, Q. Zhang, L. Gu, X. Liu, X. Wen, D. Ma, L.-Z. Wu, C.-H. Tung, T. Zhang, *Adv. Mater.* **2018**, *30*, 1803127.
[104] W. Gao, R. Gao, Y. Zhao, M. Peng, C. Song, M. Li, S. Li, J. Liu, W. Li, Y. Deng, M. Zhang, J. Xie, G. Hu, Z. Zhang, R. Long, X.-D. Wen, D. Ma, *Chem* **2018**, *doi.org/10.1016/j.chempr.2018.09.017*.
[105] F. Sastre, M. Oteri, A. Corma, H. Garcia, *Energy Environ. Sci.* **2013**, *6*, 2211.
[106] X. Lin, K. Yang, R. Si, X. Chen, W. Dai, X. Fu, *Appl. Catal. B: Environ.* **2014**, *147*, 585.
[107] X. Lin, L. Lin, K. Huang, X. Chen, W. Dai, X. Fu, *Appl. Catal. B: Environ.* **2015**, *168-169*, 416.
[108] L. Wang, Y. Zhang, X. Gu, Y. Zhang, H. Su, *Catal. Sci. Technol.* **2018**, *8*, 601.

[109] Y. Kohno, T. Tanaka, T. Funabiki, S. Yoshida, *Chem. Commun.* **1997**, 841.
[110] Y. Kohno, T. Tanaka, T. Funabiki, S. Yoshida, *J. Chem. Soc., Faraday Trans.* **1998**, *94*, 1875.
[111] Y. Kohno, T. Tanaka, T. Funabiki, S. Yoshida, *Phys. Chem. Chen. Phys.* **2000**, *2*, 2635.
[112] Y. Kohno, H. Ishikawa, T. Tanaka, T. Funabiki, S. Yoshida, *Phys. Chem. Chen. Phys.* **2001**, *3*, 1108.
[113] K. Teramura, T. Tanaka, H. Ishikawa, Y. Kohno, T. Funabiki, *J. Phys. Chem. B* **2004**, *108*, 346.
[114] K. Teramura, H. Tsuneoka, T. Shishido, T. Tanaka, *Chem. Phys. Lett.* **2008**, *467*, 191.
[115] K. Teramura, S.-i. Okuoka, H. Tsuneoka, T. Shishido, T. Tanaka, *Appl. Catal. B: Environ.* **2010**, *96*, 565.
[116] M. Tahir, N. S. Amin, *Appl. Catal. A: Gen.* **2015**, *493*, 90.
[117] M. Tahir, N. S. Amin, *Chem. Eng. J.* **2016**, *285*, 635.
[118] L. B. Hoch, T. E. Wood, P. G. O'Brien, K. Liao, L. M. Reyes, C. A. Mims, G. A. Ozin, *Adv. Sci.* **2014**, *1*, 1400013.
[119] L. B. Hoch, L. He, Q. Qiao, K. Liao, L. M. Reyes, Y. Zhu, G. A. Ozin, *Chem. Mater.* **2016**, *28*, 4160.
[120] L. He, T. E. Wood, B. Wu, Y. Dong, L. B. Hoch, L. M. Reyes, D. Wang, C. Kübel, C. Qian, j. Jia, K. Liao, P. G. O'Brien, A. Sandhel, J. Y. Y. Loh, P. Szymanski, N. P. Kherani, T. C. Sum, C. A. Mims, G. A. Ozin, *ACS Nano* **2016**, *10*, 5578.
[121] L. B. Hoch, P. G. O'Brien, A. Jelle, A. Sandhel, D. D. Perovic, C. A. Mims, G. A. Ozin, *ACS nano* **2016**, *10*, 9017.
[122] K. K. Ghuman, L. B. Hoch, P. Szymanski, J. Y. Y. Loh, N. P. Kherani, M. A. El-Sayed, G. A. Ozin, C. V. Singh, *J. Am. Chem. Soc.* **2016**, *138*, 1206.
[123] L. B. Hoch, P. Szymanski, K. K. Ghuman, L. He, K. Liao, Q. Qiao, L. M. Reyes, Y. Zhu, M. A. El-Sayed, C. V. Singh, G. A. Ozin, *Proc. Natl. Acad. Sci. USA* **2016**, *113*, E8011.
[124] Y. Dong, K. K. Ghuman, R. Popescu, P. N. Duchesne, W. Zhou, J. Y. Y. Loh, A. A. Jelle, J. Jia, D. Wang, X. Mu, C. Kübel, L. Wang, L. He, M. Ghoussoub, Q. Wang, T. E. Wood, L. M. Reyes, P. Zhang, N. P. Kherani, C. V. Singh, G. A. Ozin, *Adv. Sci.* **2018**, *5*, 1700732.
[125] M. Shao, L. Cheng, X. Zhang, D. D. D. Ma, S.-t. Lee, *J. Am. Chem. Soc.* **2009**, *131*, 17738.
[126] W. Sun, C. Qian, L. He, K. K. Ghuman, A. P. Y. Wong, J. Jia, A. A. Jelle, P. G. O'Brien, L. M. Reyes, T. E. Wood, A. S. Helmy, C. A. Mims, C. V. Singh, G. A. Ozin, *Nat. Commun.* **2016**, *7*, 12553.
[127] P. Zhang, T. Wang, J. Gong, *Adv. Mater.* **2015**, *27*, 5328.
[128] S. Linic, P. Christopher, D. B. Ingram, *Nat. Mater.* **2011**, *10*, 911.
[129] C. Wang, O. Ranasingha, S. Natesakhawat, P. R. Ohodnicki, M. Andio, J. P. Lewis, C. Matranga, *Nanoscale* **2013**, *5*, 6968.
[130] A. A. Upadhye, I. Ro, X. Zeng, H. J. Kim, I. Tejedor, M. A. Anderson, J. A. Dumesic, G. W. Huber, *Catal. Sci. Technol.* **2015**, *5*, 2590.
[131] I. Ro, C. Sener, T. M. Stadelman, M. R. Ball, J. M. Venegas, S. P. Burt, I. Hermans, J. A. Dumesic, G. W. Huber, *J. Catal.* **2016**, *344*, 784.
[132] I. Ro, R. Carrasquillo-Flores, J. A. Dumesic, G. W. Huber, *Appl. Catal. A: Gen.* **2016**, *521*, 182.
[133] X. Meng, T. Wang, L. Liu, S. Ouyang, P. Li, H. Hu, T. Kako, H. Iwai, A. Tanaka, J. Ye, *Angew. Chem., Int. Ed.* **2014**, *53*, 11478.
[134] H. Zhang, T. Wang, J. Wang, H. Liu, T. D. Dao, M. Li, G. Liu, X. Meng, K. Chang, L. Shi, T. Nagao, J. Ye, *Adv. Mater.* **2016**, *28*, 3703.
[135] J. Jia, Paul G. O'Brien , L. He, Q. Qiao, F. Teng, L. M. Reyes, T. E. Burrow, Y. Dong, K. Liao, M. Varela, S. J. Pennycook, M. Hmadeh, A. S. Helmy, N. P. Kherani, D. D. Perovic, G. A. Ozin, *Adv. Sci.* **2016**, *3*, 1600189.
[136] M. W. Knight, N. S. King, L. Liu, H. O. Everitt, P. Nordlander, N. J. Halas, *ACS Nano* **2014**, *8*, 834.
[137] H. Robatjazi, H. Zhao, D. F. Swearer, N. J. Hogan, L. Zhou, A. Alabastri, M. J. McClain, P. Nordlander, N. J. Halas, *Nat. Commun.* **2017**, *8*, 27.
[138] K. R. Thampi, J. Kiwi, M. Grätzel, *Nature* **1987**, *327*, 506.
[139] J. Melsheimer, W. Guo, D. Ziegler, M. Wesemann, R. Schlögl, *Catal. Lett.* **1991**, *11*, 157.
[140] P. G. O'Brien, A. Sandhel, T. E. Wood, A. A. Jelle, L. B. Hoch, D. D. Perovic, C. A. Mims, G. A. Ozin, *Adv. Sci.* **2014**, *1*, 1400001.
[141] G. A. Ozin, *Adv. Mater.* **2015**, *27*, 1957.
[142] J. Ren, S. Ouyang, H. Xu, X. Meng, T. Wang, D. Wang, J. Ye, *Adv. Energy Mater.* **2017**, *7*, 1601657.
[143] X. Zhang, X. Li, D. Zhang, N. Q. Su, W. Yang, H. O. Everitt, J. Liu, *Nat. Commun.* **2017**, *8*, 14542.
[144] N. Ahmed, Y. Shibata, T. Taniguchi, Y. Izumi, *J. Catal.* **2011**, *279*, 123.
[145] N. Ahmed, M. Morikawa, Y. Izumi, *Catal. Today* **2012**, *185*, 263.
[146] M. Morikawa, N. Ahmed, Y. Yoshida, Y. Izumi, *Appl. Catal. B: Environ.* **2014**, *144*, 561.
[147] M. Morikawa, Y. Ogura, N. Ahmed, S. Kawamura, G. Mikami, S. Okamoto, Y. Izumi, *Catal. Sci. Technol.* **2014**, *4*, 1644.
[148] S. Kawamura, M. C. Puscasu, Y. Yoshida, Y. Izumi, G. Carja, *Appl. Catal. A: Gen.* **2015**, *504*, 238.
[149] L. Wang, M. Ghoussoub, H. Wang, Y. Shao, W. Sun, A. A. Tountas, T. E. Wood, H. Li, J. Y. Y. Loh, Y. Dong, M. Xia, Y. Li, S. Wang, J. Jia, C. Qiu, C. Qian, N. P. Kherani, L. He, X. Zhang, G. A. Ozin, *Joule* **2018**, *2*, 1369.
[150] W. Zhang, L. Wang, K. Wang, M. U. Khan, M. Wang, H. Li, J. Zeng, *Small* **2017**, *13*, 1602583.
[151] G. Chen, R. Gao, Y. Zhao, Z. Li, G. I. N. Waterhouse, R. Shi, J. Zhao, M. Zhang, L. Shang, G. Sheng, X. Zhang, X. Wen, L. Z. Wu, C. H. Tung, T. Zhang, *Adv. Mater.* **2018**, *30*, 1704663.
[152] L. Liu, A. V. Puga, J. Cored, P. Concepción, V. Pérez-Dieste, H. García, A. Corma, *Appl. Catal. B: Environ.* **2018**, *235*, 186.
[153] S. L. Kaliaguine, B. N. Shelimov, V. B. Kazansky, *J. Catal.* **1978**, *55*, 384.
[154] M. Graetzel, K. R. Thampi, J. Kiwi, *J. Phys. Chem.* **1989**, *93*, 4128.
[155] C. F. Lien, M. T. Chen, Y. F. Lin, J. L. Lin, *J. Chin. Chem. Soc.* **2004**, *51*, 37.
[156] V. Krishna, V. S. Kamble, P. Selvam, N. M. Gupta, *Catal. Lett.* **2004**, *98*, 113.
[157] V. Krishna, V. S. Kamble, N. M. Gupta, P. Selvam, *J. Phys. Chem. C* **2008**, *112*, 15832.
[158] X. Chen, Y. Li, X. Pan, D. Cortie, X. Huang, Z. Yi, *Nat. Commun.* **2016**, *7*, 12273.
[159] M. Griitzel, *Nature* **1987**, *327*, 11.
[160] N. Ahmed, Y. Shibata, T. Taniguchi, Y. Izumi, *J. Catal.* **2011**, *279*, 123.
[161] F. Sastre, A. V. Puga, L. Liu, A. Corma, H. García, *J. Am. Chem. Soc.* **2014**, *136*, 6798.
[162] P. G. O'Brien, A. Sandhel, T. E. Wood, A. A. Jelle, L. B. Hoch, D. D. Perovic, C. A. Mims, G. A. Ozin, *Adv. Sci.* **2014**, *1*, 1400001.
[163] W. Sun, C. Qian, L. He, K. K. Ghuman, A. P. Wong, J. Jia, A. A. Jelle, P. G. O'Brien, L. M. Reyes, T. E. Wood, *Nat. Commun.* **2016**, *7*.
[164] M. Li, P. Li, K. Chang, T. Wang, L. Liu, Q. Kang, S. Ouyang, J. Ye, *Chem. Commun.* **2015**, *51*, 7645.
[165] J. Jia, P. G. O'Brien, L. He, Q. Qiao, T. Fei, L. M. Reyes, T. E. Burrow, Y. Dong, K. Liao, M. Varela, S. J. Pennycook, M. Hmadeh, A. S. Helmy, N. P. Kherani, D. D. Perovic, G. A. Ozin, *Adv. Sci.* **2016**, *3*, 1600189.
[166] H. Zhang, T. Wang, J. Wang, H. Liu, T. D. Dao, M. Li, G. Liu, X. Meng, K. Chang, L. Shi, T. Nagao, J. Ye, *Adv. Mater.* **2016**, *28*, 3703.
[167] J. Ren, S. Ouyang, H. Xu, X. Meng, T. Wang, D. Wang, J. Ye, *Adv. Energy Mater.* **2016**, 1601657.
[168] L. Lin, K. Wang, K. Yang, X. Chen, X. Fu, W. Dai, *Appl. Catal. B: Environ.* **2017**, *204*, 440.
[169] D. Mateo, J. Albero, H. Garcia, *Energy Environ. Sci.* **2017**, *10*, 2392.
[170] K. Wada, H. Yamada, Y. Watanabe, T.-a. Mitsudo, *J. Chem. Soc., Faraday Trans.* **1998**, *94*, 1771.
[171] H. H. López, A. Martínez, *Catal. Lett.* **2002**, *83*, 37.
[172] K. R. Thampi, J. Kiwi, M. Grätzel, *Catal. Lett.* **1988**, *1*, 109.
[173] M. D. Ward, J. F. Brazdil, S. P. Mehandru, A. B. Anderson, *J. Phys. Chem.* **1987**, *91*, 6515.
[174] K. Villa, S. Murcia-López, T. Andreu, J. R. Morante, *Appl. Catal. B: Environ.* **2015**, *163*, 150.
[175] K. Villa, S. Murcia-López, J. R. Morante, T. Andreu, *Appl. Catal. B: Environ.* **2016**, *187*, 30.
[176] S. Murcia-López, K. Villa, T. Andreu, J. R. Morante, *ACS Catal.* **2014**, *4*, 3013.
[177] J. Xie, R. Jin, A. Li, Y. Bi, Q. Ruan, Y. Deng, Y. Zhang, S. Yao, G. Sankar, D. Ma, J. Tang, *Nat. Catal.* **2018**, *1*, 889.
[178] C. E. Taylor, R. P. Noceti, *Catal. Today* **2000**, *55*, 259.
[179] C. E. Taylor, *Catal. Today* **2003**, *84*, 9.
[180] H. Song, X. Meng, Z.-j. Wang, Z. Wang, H. Chen, Y. Weng, F. Ichihara, M. Oshikiri, T. Kako, J. Ye, *ACS Catal.* **2018**, *8*, 7556.
[181] Y. Kato, H. Yoshida, T. Hattori, *Chem. Commun.* **1998**, 2389.
[182] L. Yuliati, M. Tsubota, A. Satsuma, H. Itoh, H. Yoshida, *J. Catal.* **2006**, *238*, 214.
[183] Y. Kato, N. Matsushita, H. Yoshida, T. Hattori, *Catal. Commun.* **2002**, *3*, 99.
[184] H. Yoshida, M. G. Chaskar, Y. Kato, T. Hattori, *J. Photochem. Photobiol., A* **2003**, *160*, 47.
[185] L. Yuliati, T. Hamajima, T. Hattori, H. Yoshida, *J. Phys. Chem. C* **2008**, *112*, 7223.
[186] H. Yoshida, N. Matsushita, Y. Kato, T. Hattori, *J. Phys. Chem. B* **2003**, *107*, 8355.
[187] L. Yuliati, T. Hattori, H. Itoh, H. Yoshida, *J. Catal.* **2008**, *257*, 396.
[188] L. Li, G.-D. Li, C. Yan, X.-Y. Mu, X.-L. Pan, X.-X. Zou, K.-X. Wang, J.-S. Chen, *Angew. Chem., Int. Ed.* **2011**, *50*, 8299.
[189] L. Li, Y.-Y. Cai, G.-D. Li, X.-Y. Mu, K.-X. Wang, J.-S. Chen, *Angew. Chem., Int. Ed.* **2012**, *51*, 4702.
[190] G. Chen, Y. Zhao, L. Shang, G. I. N. Waterhouse, X. Kang, L. Z. Wu, C. H. Tung, T. Zhang, *Adv. Sci.* **2016**, *3*, 1500424.
[191] L. Li, S. Fan, X. Mu, Z. Mi, C.-J. Li, *J. Am. Chem. Soc.* **2014**, *136*, 7793.
[192] H. Liu, X. Meng, T. D. Dao, H. Zhang, P. Li, K. Chang, T. Wang, M. Li, T. Nagao, J. Ye, *Angew. Chem., Int. Ed.* **2015**, *54*, 11545.
[193] B. László, K. Baán, E. Varga, A. Oszkó, A. Erdőhelyi, Z. Kónya, J. Kiss, *Appl. Catal. B: Environ.* **2016**, *199*, 473.
[194] H. Liu, M. Li, T. D. Dao, Y. Liu, W. Zhou, L. Liu, X. Meng, T. Nagao, J. Ye, *Nano Energy* **2016**, *26*, 398.

[195] H. Song, X. Meng, T. D. Dao, W. Zhou, H. Liu, L. Shi, H. Zhang, T. Nagao, T. Kako, J. Ye, *ACS Appl. Mater. Inter.* **2018**, *10*, 408.
[196] M. Mao, Q. Zhang, Y. Yang, Y. Li, H. Huang, Z. Jiang, Q. Hu, X. Zhao, *Green Chem.* **2018**, *20*, 2857.
[197] H. Liu, T. D. Dao, L. Liu, X. Meng, T. Nagao, J. Ye, *Appl. Catal. B: Environ.* **2017**, *209*, 183.
[198] Y. Sun, T. Ritchie, S. S. Hla, S. McEvoy, W. Stein, J. H. Edwards, *J. Nat. Gas Chem.* **2011**, *20*, 568.
[199] H. Huang, M. Mao, Q. Zhang, Y. Li, J. Bai, Y. Yang, M. Zeng, X. Zhao, *Adv. Energy Mater.* **2018**, 1702472.
[200] H. Yue, Y. Zhao, X. Ma, J. Gong, *Chem. Soc. Rev.* **2012**, *41*, 4218.
[201] S. Xie, Z. Shen, J. Deng, P. Guo, Q. Zhang, H. Zhang, C. Ma, Z. Jiang, J. Cheng, D. Deng, Y. Wang, *Nat. Commun.* **2018**, *9*, 1181.
[202] Z. Shen, S. Xie, W. Fan, Q. Zhang, Z. Xie, W. Yang, Y. Wang, J. Lin, X. Wu, H. Wan, Y. Wang, *Catal. Sci. Technol.* **2016**, *6*, 6485.
[203] S. Xie, Z. Shen, H. Zhang, J. Cheng, Q. Zhang, Y. Wang, *Catal. Sci. Technol.* **2017**, *7*, 923.

Biographies

Guangbo Chen received his BS degree (2013) and master's degree (2016) in Chemistry from Northwest University. During 2014-2016, he studied as a joint master student under the supervision of Prof. Tierui Zhang at Technical Institute of Physics and Chemistry, Chinese Academy of Sciences. He is currently pursuing his PhD at Department of Chemistry and Food Chemistry, Technische Universität Dresden (Germany). His research focuses on the development of novel nanomaterials for energy conversion applications.

Prof. Geoffrey I.N. Waterhouse completed a PhD in Chemistry at the University of Auckland in 2003. He is a Fellow of the New Zealand Institute of Chemistry, a Principal Investigator in the MacDiarmid Institute (a New Zealand CoRE) and a Chair Professor of both the South China University of Technology and Shandong Agricultural University. His research interests include solar energy capture technologies, photocatalysis, photonic band gap materials, and biosensors.

Prof. Tierui Zhang is a full professor at the Technical Institute of Physics and Chemistry, Chinese Academy of Sciences. He obtained his PhD degree in Chemistry in 2003 at Jilin University, China. He then worked as a postdoctoral researcher in the labs of Prof. Markus Antonietti, Prof. Charl F.J. Faul, Prof. Hicham Fenniri, Prof. Z. Ryan Tian, Prof. Yadong Yin, and Prof. Yushan Yan. His current scientific interests focus on catalytic nanomaterials for energy conversion.

10.1002/anie.201814313

Table of Contents

REVIEW

This review highlights recent achievements in solar-driven C1 chemistry, especially in processes such as solar-driven FTs, WGS, CO_2 hydrogenation, CH_4 and CH_3OH conversion. Particular emphasis is placed on the rational design of catalysts, structure-reactivity relationships as well as reaction mechanisms during the solar-driven processes.

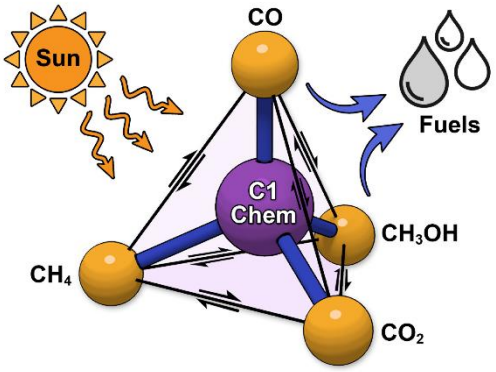

*G. Chen, G. I.N. Waterhouse, R. Shi, J. Zhao, Z. Li, L-Z. Wu, C-H. Tung, and T. Zhang**

Page No. – Page No.

Solar-to-Fuels: Recent Advances in Light-driven C1 Chemistry